Forward Genetic ENU Mutagenesis Screen for Mouse Models of Chronic Fatigue Identifies a Novel Mutation in *Slc2a4* (GLUT4)

Short Title: Chronic Fatigue Screen Identifies *Scl2a4* Mutation

Marleen H. M. de Groot[a,b], Carlos M. Castorena[c], Vivek Kumar[a,1], Jennifer A. Mohawk[a,b], Newaz I. Ahmed[c], and Joseph S. Takahashi[a,b,2]

[a]Department of Neuroscience, University of Texas Southwestern Medical Center, Dallas, TX 75390-9111
[b]Howard Hughes Medical Institute, University of Texas Southwestern Medical Center, Dallas, TX 75390-9111
[c]Department of Internal Medicine, Division of Hypothalamic Research, University of Texas Southwestern Medical Center, Dallas, TX 75390-9111
[1]Present Address: The Jackson Laboratory, Bar Harbor, ME 04609

[2]To whom correspondence should be addressed:
Dr. Joseph S. Takahashi
HHMI, Department of Neuroscience
University of Texas Southwestern Medical Center
5323 Harry Hines Blvd., NA4.118
Dallas, TX 75390-9111 USA
Tel: (214) 648-1876
Fax: (214) 648-1801
joseph.takahashi@utsouthwestern.edu

Keywords: mutagenesis screen, fatigue, GLUT4, mouse model, sleep, voluntary wheel-running activity

ABSTRACT

In a screen of voluntary wheel running to identify genetic models of chronic fatigue in ENU mutagenized C57BL/6J mice, we discovered two lines showing aberrant activity. Both lines stem from a single founder identified in a body-weight screen. Affected mice showed lower daily activity levels and low amplitude circadian rhythms with a modestly longer free-running period. Their activity was not consolidated and was interrupted with periods of inactivity throughout the night. Both the low body weight and behavioral phenotypes showed a recessive heritance pattern. These phenotypes showed linkage to a locus on chromosome 11, containing a single point mutation in the *Slc2a4* gene encoding the GLUT4 insulin-responsive glucose transporter. The single nucleotide change (A to T) in exon 10 results in a premature stop (Y440*). To our knowledge, this is the first time a mutation in this gene has been shown to result in extensive changes in general behavioral patterns.

INTRODUCTION

Fatigue is a debilitating symptom comorbid with many disorders and disease states, and may also present without readily identifiable associated disorders, the latter referred to as idiopathic fatigue (Jason et al., 2010). Fatigue persisting 6 months or more is considered chronic fatigue and if additional criteria are met, a diagnosis of Chronic Fatigue Syndrome (CFS) can be made (Fukuda et al., 1994; Wessely, 1998; Ranjith, 2005). The Centers for Disease Control and Prevention define chronic fatigue syndrome as “a debilitating and complex disorder characterized by intense fatigue that is not

23 improved by bed rest and that may be worsened by physical activity or mental exertion".
24 Fatigue is associated with increased disability, impaired functioning and increased
25 mortality (Hardy and Studenski, 2008b; Hardy and Studenski, 2008a; Moreh et al.,
26 2010). Its negative impact on activity and overall quality of life further increases the
27 need for adequate and effective treatment, although this has remained elusive.

28 The development of appropriate animal models to study the underlying
29 mechanisms of fatigue is crucial, but is hampered by the lack of a widely accepted
30 operational definition of fatigue (Maes and Twisk, 2010; Harrington, 2012). Currently
31 there are several different types of mouse models, including those based on forced
32 activity (e.g., treadmill or swimming), neurodegenerative disorders (e.g., Parkinson's or
33 Huntington's disease), cancer and its treatments, or aging, but by far the most common
34 types of models involve fatigue following an immune challenge (e.g., those mimicking
35 viral or parasitic infection) (Ottenweller et al., 1998; Anisman et al., 2008; Kudo et al.,
36 2011a; Kudo et al., 2011b; Nakamura et al., 2011; Ray et al., 2011; Bonsall et al.,
37 2015). A commonality shared by all of these model systems is a resulting alteration of
38 behavioral output, such as voluntary wheel running (Harrington, 2012).

39 The mouse is an ideal model organism to investigate physiological and
40 neurological pathways involved in fatigue (Lightfoot, 2011; Harrington, 2012). Although
41 the psychological and emotional aspects of fatigue may be somewhat difficult to study in
42 mice, the behavioral components are more readily comparable. Models based on
43 reduced or altered voluntary wheel-running activity mimic the reduced voluntary physical
44 activity exhibited by humans with fatigue. Wheel running is a robust behavior in rodents,

45 and is amenable to quantitative analysis (Shimomura et al., 2001; Siepka and
46 Takahashi, 2005b; Lightfoot, 2011). Some characteristics that may imply fatigue in mice
47 when tested on running wheels include reduced daily amount of activity, changes in
48 pattern or day-night distribution, a lack of consolidated running with an increase in the
49 number of distinct bouts, or a delayed onset or shortened duration of the daily active
50 phase.

51 There is some indication that there are genetic components related to the
52 development and manifestation of fatigue (Schur et al., 2007; Landmark-Hoyvik et al.,
53 2010; Sprangers et al., 2014; Wang et al., 2017). Polymorphisms in several human
54 candidate genes (e.g., the adrenergic receptor a1 (ADRA1A), the serotonin transporter
55 (5-HTT or SLC6A4) or receptor (HTR2A), tyrosine hydroxylase (TH), corticosteroid-
56 binding globulin (CBG), corticotropin releasing hormone receptor 1 (CRHR1), the
57 cytokine IL-1B, neuronal PAS domain protein 2 (NPAS2), the nuclear receptor subfamily
58 3; group C, member 1 glucocorticoid receptor (NR3C1), and the glutamate receptor -
59 ionotropic kinase 2 (GRIK2)) have been linked to both the occurrence and severity of
60 fatigue symptomology (Narita et al., 2003; Torpy and Ho, 2007; Collado-Hidalgo et al.,
61 2008; Lin and Huang, 2008; Smith et al., 2008; Smith et al., 2011; Johnston et al.,
62 2016). A study comparing chronic fatigue syndrome patients to healthy controls using a
63 single nucleotide polymorphism (SNP) chip with over 900,000 SNPs identified 442
64 candidates associated with chronic fatigue syndrome, and highlighted two genes never
65 before associated with fatigue (C-type lectin domain family 4, member M (CLEC4M) and
66 coiled-coil domain containing 157 protein (CCDC157)) (Schlauch et al., 2016). In

67 addition, mice with mutations in several genes have shown phenotypes consistent with
68 fatigue (e.g., corticosteroid-binding globulin (CBG), recombinase activating gene 2
69 (RAG2), and interleukin-10 (IL-10)) (Petersen et al., 2006; Golumbek et al., 2007;
70 Krzyszton et al., 2008).

71 We know that random mutagenesis paired with forward genetic screening has
72 proven invaluable in establishing and expanding understanding of gene function (Justice
73 et al., 1999; Soewarto et al., 2000; Keays and Nolan, 2003; Clark et al., 2004; Goldowitz
74 et al., 2004; Cordes, 2005; Vitaterna et al., 2006; Kumar et al., 2011; Moresco et al.,
75 2013). In the field of circadian rhythms, forward genetics has been a powerful tool for
76 identifying both clock and clock-controlled genes (Takahashi et al., 2008). We
77 systematically screen randomly mutagenized mice on running wheels in search of lines
78 exhibiting alterations in voluntary wheel-running activity. We believe that the
79 identification of mouse lines that harbor mutations resulting in altered behavioral
80 patterns consistent with chronic fatigue, and the subsequent identification of the
81 responsible gene(s) or pathways, will contribute significantly to our understanding of the
82 pathophysiology of this debilitating disorder.

83 As part of a larger phenotype-driven ENU mouse mutagenesis project (Siepka
84 and Takahashi, 2005a), we screened mice for abnormalities in the expression of
85 voluntary wheel-running activity, with the hope of identifying genes involved in
86 behavioral chronic fatigue. We describe the identification of two independent lines of
87 mice stemming from a single mutagenized founder showing profound alterations in
88 amount, pattern and distribution of daily wheel running resulting from a single point

mutation (*twiggy*; MGI:5805978) in *Slc2a4* encoding the insulin-responsive glucose transporter, GLUT4. To our knowledge, this is the first description of impaired functioning of this gene resulting in extensive behavioral abnormalities. The finding that a mutation in this gene results in widespread behavioral modifications and altered expression of daily activity patterns indicates that its role is likely more diverse than has previously been appreciated.

RESULTS

Mice show abnormal, low amplitude voluntary wheel-running activity patterns.

In a voluntary wheel-running screen designed to isolate mice with heritable abnormal patterns of behavior, we identified two lines of mice showing abnormal activity consistent with chronic fatigue (Fig. 1). These two lines both stemmed from a single, third generation (G3) founder female identified as having low body weight (Fig. S1 A), which we named '*twiggy*' and which was backcrossed to wildtype C57BL/6J to produce N2 progeny (Fig. S1 B). Two additional G3 pedigrees stemming from the same mutagenized founder (G0) male also contained affected G3 mice with low body weight (2 out of 8 mice and 3 out of 26 mice, respectively) but none of these G3s produced enough offspring for heritability testing. N2 progeny of the *twiggy* G3 founder female showed body weights within the normal range, but an intercross of N2 mice produced a subset (~5-8 out of 57) that showed the low body-weight phenotype (Fig. S1B). A subsequent backcross of affected N2F2 mice to wildtype C57BL/6J produced N3 progeny that were unaffected, indicating that this phenotype is expressed in a non-sex-

111 linked, recessive heritance pattern. Despite the low body-weight phenotype and overall
112 smaller appearance, affected animals were completely healthy, and there was no
113 observed effect on reproductive fitness.

114 Mice were maintained in two distinct lines following initial heritability testing (Fig.
115 S1 C and D; Table S1). The first is a backcross/intercross (B/Int-x) line generated and
116 maintained by backcrossing affected (presumably homozygous) mice to C57BL/6J, and
117 then intercrossing the resulting offspring, producing alternating generations of obligate
118 heterozygous carrier "B/Int-x (N#)" mice, and "B/Int-x (N#F2)" mice of all 3 possible
119 genotypes (+/+, +/m, and m/m; ~25%, ~50% and ~25%, respectively; Fig. S1 C and D –
120 left panels; Table S1; where N# denotes the number of backcross generations). The
121 second is an incross (I-x) line generated and maintained by crossing affected siblings
122 with each other over successive generations beginning with the first N2F2 progeny
123 shown in Fig. S1 B, to produce a homozygous line (Fig. S1 C and D – right panels). The
124 body weights of 8 sequential generations of each line are shown in Fig. S1 C (males)
125 and D (females), and, while all 8 I-x generations show body weights lower than the
126 screening mean, mice in the B/Int-x show a distinct generation-alternating pattern of
127 results.

128 Because of the low body weight, we measured fasting blood glucose from
129 individuals of both the B/Int-x and I-x lines. Although body weights following a 4h fast
130 were significantly lower for both males and females of the I-x line than those of the B/Int-
131 x line (Fig. S1 E), there was no significant difference between the two lines in fasting
132 blood glucose (Fig. S1 F). Values for all mice tested were within the normal blood

133 glucose range for C57BL/6J mice reported by Jackson Labs (Center for Genome
134 Dynamics; CGDpheno1 glucose (plasma GLU, 4h fast); phenome.jax.org).
135 When mice stemming from these lines were housed in cages with free access to
136 a running wheel, a number of mice in the B/Int-x (N6F2) line showed a hypoactive and
137 disrupted pattern of voluntary wheel-running activity (Fig. 1 A and B). Representative
138 activity plots (actograms) of two mice of the B/Int-x (N6F2) line are shown, with one
139 exhibiting normal levels and patterns of activity (Fig. 1 A) and one showing the abnormal
140 phenotype (Fig. 1 B). In contrast, all the mice in the I-x (N2F10) line showed this same
141 aberrant pattern (Fig. 1 C and D), consisting of low activity levels, increased bouts of
142 activity during the light or rest phase, non-consolidated or disrupted nocturnal activity,
143 and irregular onsets of the main nocturnal bout. When affected mice from the I-x
144 (N2F10) line were backcrossed to C57BL/6J mice in a test cross (T-x (N3); Table S1),
145 none of the progeny showed the phenotype, and circadian, or daily, wheel-running
146 behavior was indistinguishable from that of wildtype mice (Fig. 1 E). Average waveforms
147 of 10 days of recording under a light-dark (LD) cycle clearly show that overall wheel-
148 running activity levels are significantly decreased in mice of the I-x (N2F10) line (Fig. 1
149 F). The B/Int-x (N6F2) line included some mice that showed the phenotype and some
150 that didn't, whereas none of the T-x (N3) mice were affected, and these showed a
151 normal circadian pattern of activity with high levels of nocturnal wheel running.
152 Quantification of total activity (Fig. 1 G), light phase activity (Fig. 1 H), and
153 number of activity bouts per day (Fig. 1 I) recorded during the LD cycle, showed
154 significant differences among progeny of the three types of crosses, with mice of the I-x

155 (N2F10) line showing low activity, with higher levels of activity during the rest phase and
156 higher numbers of distinct activity bouts. Differences in activity levels were maintained
157 when mice were recorded in constant darkness (DD; Fig. 1 J), and the amplitude of the
158 wheel running rhythm in affected mice was significantly lower than in unaffected mice
159 (Fig. 1 K). The period of the free-running circadian rhythm recorded in DD was
160 significantly longer for mice of the I-x (N2F10) line (Fig. 1 L), although these values fall
161 within the normal range for wildtype C57BL/6J (Shimomura et al., 2001).
162
163 **Frequent rest bouts interrupt nocturnal wheel-running activity in affected mice.**
164 In order to characterize further the abnormal behavioral pattern these mice exhibit, we
165 assessed their behavioral profiles during the dark phase using both time-lapsed
166 photography (Fig. 2) and video recording (Fig. 3). Images captured once every min for
167 15h beginning at the start of the dark phase for 3 individual wildtype C57BL/6J (Fig. S2)
168 and 5 individual I-X (N2F14) mice (Fig. S3) were scored on a range of 9 behavioral
169 states. The I-X (N2F14) mice were each recorded twice, with one week occurring
170 between recording sessions (Fig. S3). The ethogram of scored behaviors for the
171 representative wildtype C57BL/6J mouse shows extended bouts of wheel running with
172 short interruptions for drinking, eating, and general cage activity (Fig. 2 A). This mouse
173 only adopted a body posture consistent with sleep during the end of the end of the dark
174 phase (i.e., after 3:00 h). The amount of time spent in the various behaviors for the first
175 6h of the dark phase (18:00 – 0:00 h) are represented in a pie chart for this individual
176 mouse in Fig. 2 C and averaged for all 3 wildtype mice in Fig. 2 D. The pattern of

177 behaviors shown by the representative I-x (N2F14) mouse (Fig. 2 B) does not resemble
178 that recorded for wildtype mice. Consolidated, extended bouts of wheel running are
179 absent, and running is interrupted with periods of time when the mouse is near the
180 wheel, but is not active. During these periods of time, the mouse is seen to adopt a low,
181 crouched posture indicative of sleep (Fig. 2 G – right panel). The distribution of
182 behaviors for the first 6h of the dark phase (18:00 – 0:00 h) for this mouse is shown in
183 Fig. 2 E, and for all 5 I-x (N2F14/15) mice recorded twice in Fig. 2 F. Most notably,
184 running is significantly decreased for these mice compared to wildtype (Fig. 2 C-F),
185 Even more surprising, all 5 I-X (N2F14/15) mice show sleep postures during this 6h time
186 period on both recording sessions, whereas wildtype mice were never observed to do
187 this (Fig. S2 and S3).
188 Videos recorded during the first few hours of the dark phase for three individual
189 mice of the I-x (N2F21) and T-x (N11F3) generations were scored and the data are
190 plotted along with those for two unaffected T-x (N3F2) mice (Fig. 3 A and B). Mice of
191 both affected groups showed extremely low wheel-running levels compared to T-x
192 (N3F2) unaffected mice (Fig. 3 A and B – upper panels). The T-x (N3F2) mice never
193 showed behavioral arrest and lowered posture consistent with sleep during this time of
194 the day, whereas all three individuals of the other two lines did (Fig. 3 A and B – lower
195 panels).
196
197 **Abnormal phenotypes map to a single locus on chromosome 11.**

198 To map the mutation, we crossed affected mice from both the I-x and the B/Int-x lines to
199 C57BL/10J mice, and then intercrossed the resulting M-x (F1) progeny (n=92) to
200 produce M-x (F2) mice (Table S1). In total, 207 M-x (F2) mice from 9 independent
201 matings were produced and were tested on running wheels under LD and DD conditions
202 for the presence of the behavioral phenotype (Fig. 4). All data were compared to F1 and
203 F2 mice generated from crosses of wildtype C57BL/6J and C57BL/10J mice
204 (designated as WTB6B10F1 (n=63) and WTB6B10F2 (n=112), respectively).
205 Representative actograms recorded from two M-x (F2) mice showing the low-amplitude,
206 low activity, highly disrupted behavioral wheel-running phenotype are shown in Fig. 4 B
207 and C, with an unaffected mouse shown in Fig. 4 A. No WTB6B10F1, WTB6B10F2 or
208 M-x (F1) mouse exhibited this constellation of behavioral phenotypes, although some
209 individuals did show some of its component characteristics (e.g., low activity but no
210 increased running in the light phase or no lack of consolidation of nocturnal activity).
211 Mice of the M-x (F2) generation showed decreased activity recorded under LD (Fig. 4D)
212 and DD (Fig. 4E), increased amount of activity in the light phase (Fig. S4 A), and a
213 lower amplitude rhythm recorded in DD (Fig. 4F). There was no significant difference
214 found in number of activity bouts per day (Fig. S4 B), and the period of the free-running
215 rhythm was not altered for M-x (F2) mice, although interestingly, the WTB6B10F2 mice
216 did show a significantly shorter period (Fig. S4 C).
217 Using a genome-wide SNP panel of markers designed to differentiate C57BL/6J
218 from C57BL/10J (Table S2), the genotypes of 74 selected affected and unaffected M-x
219 (F2) mice were determined, and were assessed for linkage to the various phenotypic

220 measurements. Significant log odds ratio (LOD) peaks with linkage to a single locus on
221 chromosome 11 were found for the amount of activity recorded in LD (Fig. 4 G) and DD
222 (Fig. 4 H), and amplitude of the rhythm in DD (Fig. 4 I). No significant linkage was found
223 for the percentage of activity occurring during the light phase (Fig. S4 D and G), the
224 number of activity bouts occurring per day (Fig. S4 E and H), or the free-running period
225 in DD (Fig. S4 F and I). Activity levels in LD (Fig. 4 J), and in DD (Fig. 4 K), as well as
226 the amplitude of the rhythm in DD (Fig. 4 L), are plotted as a function of genotype at
227 SNP marker rs13481117 located on chromosome 11, position 79252230. Mice
228 homozygous for the C57BL/6J allele (designated as "B6/B6") show lower activity levels
229 in both LD and DD with a lower amplitude circadian rhythm.
230

231 **A point mutation in *Slc2a4* encoding GLUT4 is identified in affected mice.**

232 In order to identify the gene responsible for the abnormal phenotypes described, we
233 performed whole-exome sequencing (WES) of pooled DNA collected from mice of the I-
234 x (N2F20) generation, and those from a test cross stemming from affected B/Int-x
235 (N11F2) mice (T-x (N11F3); N=16 for each line). Representative activity records of mice
236 in the various generations used for this experiment are shown in Fig. S5 A-F. Body-
237 weight data collected at 8 weeks of age for both male and female mice in the I-x
238 (N2F20) and T-x (N11F3) generations, as well as for those of the B/Int-x (N11) and
239 B/Int-x (N1F2) used to produce the T-x (N11F3) mice, reveal that mice of both lines
240 chosen for WES have significantly lower body weight (Fig. S5 G). In addition, mice of
241 both presumptive homozygous lines (I-x (N2F20) and T-x (N11F3)) showed significantly

242 lower levels of activity in LD compared to mice from the B/Int-x (F1) and B/Int-x (F2)
243 generations (Fig. S5 H). Importantly, activity levels and wheel running patterns did not
244 differ between these two presumptive homozygous lines, indicating that both were, in
245 fact, homozygous for the same genetic mutation.

246 WES results revealed a single point mutation in the *Slc2a4* gene encoding
247 GLUT4, the insulin-responsive glucose transporter (Fig. 5). No other gene within the
248 linked region of chromosome 11 had polymorphisms represented in both of the samples
249 analyzed. Remarkably, all reads covering this region of the genome for both of the
250 pooled samples showed this same SNP (Fig. 5 A – red arrows). For clarity, 19
251 representative reads from each of the pooled samples are shown at higher
252 magnification (Fig. 5 A – lower panel). A single nucleotide substitution (A to T) within the
253 distal end of exon 10 of the gene results in a premature stop (Y440*; see Fig. 5 B).
254 Genotyping for this SNP revealed that all mice in the 2 test cross lines were
255 homozygous for the mutant allele of this gene, whereas mice in the B/Int-x lines showed
256 the expected Mendelian ratio of genotypes at this mutant locus. Surprisingly, western
257 blot analysis showed that homozygous mice had higher levels of protein in the
258 gastrocnemius muscle than heterozygotes and wildtype littermates (Fig. 5 C), indicating
259 that the mutation appears to result in protein accumulation or increased expression.

260 Despite the higher levels of accumulated protein, mice homozygous for the
261 *twiggy* mutation show phenotypes similar to those shown by GLUT4 knockout mice
262 (Katz et al., 1995; Gorselink et al., 2002; Simoes et al., 2004; Fueger et al., 2007; Fam
263 et al., 2012). Despite normal fasting glucose levels (Fig. 6 B and also Fig. S1 F),

264 *Slc2a4*$^{twgy/twgy}$ mice had impaired glucose clearance with significantly elevated blood
265 glucose levels 15, 30 and 45 min after glucose injection (Fig. 6 A). Both +/twgy and
266 twgy/twgy male mice showed decreased body weight, although at this age female body
267 weights did not differ significantly among genotypes (Fig. 6 C). Like GLUT4 knockout
268 mice (Katz et al., 1995), twgy/twgy of both sexes had enlarged hearts (Fig.6 D). The
269 *twiggy* mutation in *Slc2a4* resulted in impaired exercise tolerance, with twgy/twgy mice
270 showing shorter times (Fig. 6 E) and distance (Fig. 6 F) to exhaustion upon testing on a
271 treadmill. Homozygous twgy/twgy mice also had elevated blood glucose (Fig. 6 G) and
272 decreased lactate (Fig. 6 H) levels following completion of the treadmill task.
273 When mice of the B/Int-x (N12F2) line were housed with access to a running
274 wheel, only those mice with the homozygous twgy/twgy genotype showed the
275 behavioral pattern identified in the original two lines (Fig. 7 A and Fig. 1 A-D). Thus, this
276 pattern, consisting of decreased wheel-running behavior (Fig. 7 B) with a characteristic
277 non-consolidated, messy pattern of expression, an increase in activity in the light phase
278 (Fig. 7 C) and increased number of shorter, distinct bouts of activity, that is indicative of
279 an overall excessive fatigability and sleep/wake disruption, shows a clear recessive
280 mode of inheritance.
281
282 **SUMMARY AND DISCUSSION**
283 Excessive fatigue that defies simple explanation affects large subsections of the
284 population at one time or another, and results in diminished daily functioning and quality
285 of life (Wessely, 1998; Ranjith, 2005; Jason et al., 2010). It can be a symptom or side

286 effect of varied diseases and disorders and their treatments, but can also be manifest
287 independent of other comorbid diagnoses or etiologies (Morris et al., 2015; Saligan et
288 al., 2015; Skoie et al., 2015). For those persons suffering from this debilitating disorder,
289 and their loved ones, effective treatments would be most welcome, but in order for new
290 treatments to be identified and developed, informative animal models of chronic fatigue
291 are crucial. We carried out a forward genetic screen in order to identify mouse lines
292 showing behavioral characteristic of chronic fatigue. We describe the identification of a
293 novel mutation in the *Slc2a4* gene encoding GLUT4 that results in a distinct daily
294 voluntary wheel-running pattern that is consistent with chronic fatigue. Affected mice
295 homozygous for the *twiggy* mutation of *Slc2a4* show a behavioral pattern consisting of
296 low, non-consolidated and messy wheel-running activity, with increased short bursts of
297 activity interrupting the rest phase. These mice sleep during times of the day that normal
298 nocturnal wildtype mice would never sleep (i.e., during the first half of the active phase).
299 This pattern of behavior is consistent with increased fatigability, and suggests that
300 impaired functioning of the insulin-responsive glucose transporter (GLUT4), or other
301 impairments in glucose regulation and homeostasis may play a role in the underlying
302 pathophysiology of chronic fatigue.

303 Additional phenotypic characteristics observed in *Slc2a4*$^{twgy/twgy}$ homozygous
304 mice are consistent with a non-functioning GLUT4 transporter (Katz et al., 1995). These
305 characteristics include a low body weight, impaired glucose tolerance response with a
306 normal baseline fasting blood glucose level, increased heart mass consistent with
307 cardiac hypertrophy, decreased exercise tolerance, and increased fatiguing response

308 with abnormal blood glucose and lactate levels following exercise. Surprisingly, although
309 these phenotypic characteristics largely match those described for the GLUT4 null
310 mouse (Katz et al., 1995; Tsao et al., 1997; Stenbit et al., 2000; Jiang et al., 2001;
311 Gorselink et al., 2002; Simoes et al., 2004; Fueger et al., 2007), the protein levels in
312 *Slc2a4*$^{twgy/twgy}$ homozygous mice were found to be elevated, suggestive of protein
313 accumulation due to impairments in turnover or degradation of the protein, or
314 compensatory upregulation. It is possible that the mutation results in a malformation of
315 GLUT4 that interferes with its translocation or fusion to the plasma membrane, or that it
316 impairs its function as a glucose transporter. Either of these possibilities may result in a
317 compensatory over production of the protein. The premature stop introduced into exon
318 10 of the gene would likely result in the truncation of the protein and absence of the
319 carboxy terminus. There are several important regulatory elements located in this region
320 of the protein that play a role in its subcellular localization and transmission to the
321 plasma membrane in response to circulating insulin, dietary components and
322 metabolites, or exercise-related signaling pathways (Huang and Czech, 2007; Sadler et
323 al., 2013; Govers, 2014; Alvim et al., 2015; Gannon et al., 2015; Sylow et al., 2017). It
324 remains to be determined whether the phenotypes resulting from the presumably
325 truncated form of *Slc2a4* are the result of impaired functioning of the glucose transporter
326 itself, or from impairments in its vesicular localization and trafficking to the membrane in
327 response to insulin or other signaling cascades.
328 The constellation of phenotypes described for mice in the *twiggy* lines, including
329 low body weight, abnormal voluntary wheel running, and physiological alterations such

330 as enlarged hearts and impaired glucose tolerance responses, all show a clear
331 recessive heritance pattern. For virtually all phenotypes measured, heterozygous
332 *Slc2a4*$^{+/twgy}$ mice were indistinguishable from their wildtype littermates and/or wildtype
333 C57BL/6J controls. This is in sharp contrast to the GLUT4 knockout heterozygous
334 mouse that exhibits phenotypes consistent with diabetes (Rossetti et al., 1997; Stenbit
335 et al., 1997; Tsao et al., 1999; Li et al., 2000). It has been suggested that this diabetic
336 phenotype, which is manifest in only a subpopulation of the heterozygous knockouts
337 and appears to vary with age, could be an artifact of genetic background; however, this
338 remains an open issue (Stenbit et al., 1997). In addition, GLUT4 protein levels are
339 diminished in heterozygous GLUT4 knockout mice (Rossetti et al., 1997; Stenbit et al.,
340 1997; Tsao et al., 1999; Li et al., 2000). In contrast, protein levels of GLUT4 were
341 unchanged in the muscle of *Slc2a4*$^{+/twgy}$ mice. They were not diminished as in the
342 heterozygous knockout, absent as in the homozygous knockout, nor elevated as in the
343 *Slc2a4*$^{twgy/twgy}$ mice. This finding reinforces the idea that this mutation resulting in a
344 premature stop in exon 10 of the gene does not simply knock out GLUT4, and therefore
345 it represents a novel model that can be used to further characterize GLUT4 functioning.
346 The GLUT4 glucose transporter was historically considered a peripheral-acting
347 glucose channel, with expression thought to be limited to muscle, adipose tissues, and
348 heart (Charron et al., 1989; Liu et al., 1992). Recent studies have shown that it is, in
349 fact, expressed more widely and can also be found in distinct neuronal populations
350 throughout the brain in mice (Choeiri et al., 2002). This more varied expression pattern
351 and anatomical localization suggests that GLUT4 functions are more complex than

352 simply a shunt for glucose in peripheral tissues. For example, a very recent study shows
353 that GLUT4 functions to maintain neuronal, and specifically synaptic, energy
354 requirements and is essential for maintaining extended synaptic transmission (Ashrafi et
355 al., 2017). The use of conditional genetic tools has also shed more light on the diverse
356 functions of GLUT4. Interfering with insulin signaling specifically in all tissues
357 expressing GLUT4 results in a diabetic phenotype that is due, at least in part, to
358 impaired insulin signaling in neuronal populations (Lin et al., 2011). It is interesting to
359 note that these mice showed decreased body weight, but did not show any alterations in
360 activity amounts or patterns (Lin et al., 2011). Mice with GLUT4 removed selectively
361 from the brain show that neuronal GLUT4 is critical for assessing and reacting to
362 changes in blood glucose levels (Reno et al., 2017); however, it is possible that some of
363 these effects are non-specific *Cre*-driver related since Nestin-*Cre* is expressed
364 peripherally and mice carrying this transgene have been shown to have metabolic
365 phenotypes (Harno et al., 2013). Work has been initiated to try to identify the function of
366 distinct subgroups of GLUT4 neurons using methods to isolate and/or selectively ablate
367 those expressing this gene (Ren et al., 2014; Ren et al., 2015). The removal of
368 hypothalamic neurons expressing GLUT4 resulted in metabolic changes that are
369 consistent with impaired energy utilization and homeostatic processes, but did not result
370 in locomotor deficits (Ren et al., 2015). These mice ate less and lost weight, had altered
371 oxygen consumption and energy expenditure, and increased fasting blood glucose and
372 aberrant glucose tolerance responses, but the amount and daily pattern of activity
373 remained unchanged. These mice did, however, show a decreased activity response to

374 an overnight fast, and did not increase activity levels as much as unablated controls
375 (Ren et al., 2015). Clearly, the use of these genetic tools to conditionally manipulate the
376 expression of GLUT4 in anatomically and temporally controlled ways will be critical in
377 fully characterizing the function of this glucose transporter. This should allow for the
378 determination of exactly how GLUT4 removal or altered function results in the seemingly
379 varied array of phenotypic outcomes described in the literature to date.

380 The identification of a novel mutation in the *Slc2a4* gene resulting in a
381 constellation of abnormal behavioral characteristics consistent with chronic fatigue was
382 somewhat surprising, but not necessarily unexpected. It seems logical that impaired
383 glucose processing and homeostasis, with a concomitant altered tolerance of exercise,
384 would result in aberrant patterns of voluntary wheel-running activity as well. Voluntary
385 wheel running is increased in mice overexpressing GLUT4 in muscle (Tsao et al., 2001),
386 but GLUT4 expression levels did not differ between active and inactive mouse strains
387 (Dawes et al., 2014). It is likely, however, that impaired glucose transport and cellular
388 utilization would have some effect on voluntary sustained activity. Switching from
389 predominantly glucose to fatty acid fuel utilization in muscle, either by transgenic or
390 pharmacologic manipulation of the peroxisome proliferator-activated receptor delta
391 (PPARδ) pathway, increases exercise endurance in mice (Wang et al., 2004; Narkar et
392 al., 2008; Fan et al., 2017). Whether or not this increase in exercise capacity translates
393 into an increase in voluntary activity remains to be fully elucidated. For instance, mice
394 deficient in both cryptochrome 1 and 2 (Cry1/2 dKO) ran faster and for longer distances
395 than wildtype or single knockout controls on a treadmill task, presumably through de-

396 repression of PPARδ activity; however, these mice showed decreased daily voluntary
397 wheel-running behavior (Jordan et al., 2017). It remains to be determined whether or not
398 treatment of *Slc2a4*$^{twgy/twgy}$ mice with exercise mimetics would normalize some of the
399 behavioral abnormalities in wheel running that we observed (Fan and Evans, 2017).
400 This may prove informative to the investigation of how these novel pharmacological
401 treatments may apply to patients with chronic fatigue, for whom voluntary exercise
402 programs have been less than successful.

403 Fatigue, and alterations in the activity of daily living are well-described side
404 effects and symptoms of both type I and type II diabetes (Fritschi and Quinn, 2010;
405 Lasselin et al., 2012; Moulton et al., 2015). Like fatigue in other patient populations,
406 fatigue in diabetes is associated with physiological, psychological and lifestyle variables,
407 but may be exacerbated by fluctuations in blood glucose levels and homeostasis. There
408 is also some evidence suggestive of abnormal metabolic responses in chronically
409 fatigued patients, with abnormalities in energy and sugar metabolism comprising one of
410 the three main categories of pathways identified (Germain et al., 2017). The
411 identification of abnormalities in metabolic pathways in chronic fatigue, both as
412 candidates for geared treatment options, and as potential biological markers that can be
413 used to differentially diagnose various subtypes of the disorder, have received an
414 increase in scientific focus recently (Klimas et al., 2012; Maxmen, 2017).

415 Using an unbiased, forward genetic ENU mutagenesis screen for chronic fatigue,
416 we identified mice with a mutated form of the GLUT4 transporter; however, we are by no
417 means suggesting that mutations in GLUT4, or impaired glucose transport underlie all

418 manifestations of fatigue, although it may play a role in at least a subset of cases.
419 Rather, it is likely that chronic fatigue represents a persistent altered homeostatic state
420 in response to a variety of triggers and physiological adaptations (Klimas et al., 2012). It
421 is hoped that additional screening of mutagenized mouse lines for abnormalities in the
422 expression of voluntary wheel-running behavior will yield additional candidate genes
423 and pathways that are implemented in this complex disorder. In the mean time, studies
424 to determine the effectiveness of treatment strategies geared towards normalizing
425 glucose processing and transport in the *Slc2a4*^{twiggy} mice and other mouse models of
426 chronic fatigue may hold promise. In addition, assessing glucose tolerance in patients
427 for whom fatigue remains an unexplained symptom may be warranted.
428

429 **MATERIALS AND METHODS**

430 Animals and Housing

431 All mice were group housed in standard mouse cages under a 12:12 LD cycle (lights on
432 at 6:00 AM) with water and regular mouse chow (2018 Teklad Global 18% Protein
433 Rodent Diet, Envigo, Madison, WI, USA) available *ad libitum*, unless otherwise stated.
434 Mice were produced in our colony from strategic crosses, or were ordered from an in-
435 house breeding core facility (Mouse Breeding Core, Wakeland lab, UT Southwestern
436 Medical Center, Dallas, TX, USA), which orders its breeding mice from Jackson Labs
437 (Bar Harbor, ME, USA). Some wildtype C57BL/6J mice were also ordered from Jackson
438 Labs (Stock Number 000664) directly. The generation of the original ENU mutagenized
439 screening population and body weight screen were done at Northwestern University,

440 and all behavioral and subsequent phenotypic characterizations were performed at the
441 University of Texas Southwestern Medical Center. The Institutional Animal Care and
442 Use Committee (IACUC) of Northwestern University and the University of Texas
443 Southwestern Medical Center approved all animal procedures (ACUC# 2003-0034, and
444 APNs 2009-0054, 2015-100925 and 2015-101140, respectively). The Slc2a4^{twiggy} line
445 has been donated to Jackson Labs (C57BL/6J-*Slc2a4*^{twiggy}/J, Stock Number 029699).
446

447 ENU mutagenesis and Phenotypic Screening

448 The generation of N-Ethyl-N-nitrosourea (ENU; Sigma; catalog #N3385) mutagenized
449 mice and their progeny for initial high-throughput screening was described previously
450 (Siepka and Takahashi, 2005a). Briefly, male C57BL/6J mice (~6 weeks of age) were
451 injected with 250 mg/kg of ENU. Following a recovery period of ~6 weeks, these mice
452 were crossed with wildtype C57BL/6J females to produce generation 1 (G1) males
453 which were again crossed to wildtype C57BL/6J females to produce G2 females. These
454 G2 females were backcrossed to their G1 fathers to produce G3 mice of both sexes
455 used for phenotype screening.

456 More advanced generations of mice, further removed from the original G0
457 founders, were used for the more in depth behavioral phenotypic screening. Progeny of
458 selected lines of mice that were at least 8 weeks old were individually housed in
459 standard polycarbonate mouse cages (Fischer Scientific; catalog # 01-288-1B and 01-
460 288-21) containing a 4.75” diameter stainless steel running wheel placed inside isolation
461 cabinets containing 12 to 24 cages each, as described previously (Siepka and

462 Takahashi, 2005b). Temperature and humidity were monitored throughout, and the mice
463 were initially recorded under a 12:12 LD cycle (green LEDs, ~100 lux at the level of the
464 cage floor). Following the initial 3 weeks of testing under 12:12 LD, selected individual
465 progeny from specific crosses were tested under constant darkness (DD) or constant
466 light (LL) conditions. Wheel-running behavior was recorded using ClockLab Data
467 Acquisition Software (Actimetrics Inc., Wilmette, IL, USA). Wheel-running data,
468 specifically total daily amount, number of daily bouts, and percentage of activity
469 occurring in the light during LD recording, as well as total daily amount of activity, free-
470 running period, and amplitude of the rhythm recorded in DD, were quantified using
471 ClockLab Analysis Software (Actimetrics Inc., Wilmette, IL, USA). For all data
472 quantification, recording days 6-15 under LD and 31-40 under DD were used. All wheel-
473 running cages, food and water bottles were changed every 21 days.
474
475 Behavioral Time-Lapsed Photography and Video Recording
476 I-x (N2F14 and N2F15) and C57BL/6J wildtype mice were housed in individual running-
477 wheel cages as described above. Using a Sony Handycam DCR-HC62 camera with an
478 LED IR light source, photographs were taken at 1 min intervals beginning at lights off (or
479 18:00) for 15h. The resulting pictures were scored from 1 to 9 for the behavioral state or
480 cage location depicted in each. The scores used were: 1) drinking, 2) eating, 3) near the
481 food hopper, 4) on the wheel running, 5) near the wheel awake, 6) end of the cage
482 awake, 7) end of the cage resting, 8) near the wheel asleep, and 9) end of the cage

483 asleep. These scores were plotted in ethograms according to the time at which each
484 picture was taken.
485 Video recording of 3 I-x (N2F21) mice, and mice from two different test crosses
486 (T-x (N3F2) n=2 and T-x (N11F3) n=3), was done under the same IR light source
487 described above using the same Sony Handycam camera with Sony Premium Mini DV
488 Cassettes (DVM60 ME LP:90) from 20:00 to 21:30 (i.e., 2h to 3.5h into the dark phase).
489 Wheel running was recorded throughout this period as described above. The resulting
490 video was scored for behavioral arrest indicative of sleep by two researchers blind to
491 mouse identity. Periods of immobility with lowered posture lasting longer than 40
492 consecutive seconds were scored as sleep (Pack et al., 2007).
493
494 Body Weight, Fasting Blood Glucose, Health Assessment, and Tissue Collections
495 All mice produced in our colony were weighed at specific ages through development. At
496 weaning, and at regular intervals thereafter, mice were visually inspected for general
497 health and wellness. For the determination of blood glucose levels, mice were fasted for
498 4h during the middle of the light phase (a time when mice do not normally eat). Body
499 weights were measured at the beginning and the end of the 4h fast, and blood glucose
500 was determined from a small droplet of blood taken from the tip of the tail, using the
501 Precision Xtra blood glucose meters and glucose test strips (Abbott Diabetes Care Inc.,
502 Almeda, CA, USA). At the end of experiments and phenotypic characterization, mice
503 were euthanized with CO_2 followed by cervical dislocation. In some cases, tissues

504 (tailtips, spleens and hearts) were collected for weighing or DNA extraction followed by
505 genotyping.
506
507 Mapping
508 Affected mice from the I-x and B/Int-x lines were selected and crossed with wildtype
509 C57BL/10J mice (Stock Number 000665, Jackson Labs, Bar Harbor, ME, USA) to
510 produce mapping (M-x) F1 mice that were intercrossed to produce F2 progeny.
511 Additional crosses of wildtype C57BL/6J and C57BL/10J were also set up to produce
512 control (WTB6B10) F1 and F2 mice. All mice produced were individually housed in
513 running-wheel cages after 8 weeks of age and their behavior was recorded in LD (for 3
514 weeks) and DD (for 3 weeks) as described above. Following behavioral testing, mice
515 were euthanized and spleens were collected, frozen onto dry ice, and then stored at -
516 80°C. Spleen DNA from 74 selected mice (half presumptive homozygous mutants and
517 half presumptive wildtypes or heterozygotes) was extracted using phenol chloroform
518 genomic DNA extraction method. The final DNA pellet was suspended in RNAse free
519 H2O. Concentrations were determined with a NanoDrop spectrophotometer, and DNA
520 was genotyped using Taqman probes on Fluidigm platform using the 96.96 chip
521 according to manufacturer instructions as described previously (Kumar et al., 2013).
522 QTL linkage analysis was performed using R/QTL as described previously (Broman et
523 al., 2003; Kumar et al., 2013). Genotyping failed for one spleen sample, and these data
524 were subsequently removed from further analyses.
525

526 Whole Exome Sequencing

527 Test crosses (T-x) of affected, presumably homozygous B/Int-x (N11F2) were set up to
528 produce homozygous T-x (N11F3) progeny. Following phenotype recording on wheels,
529 mice were euthanized and spleens were collected from 16 representative T-x (N11F3)
530 individuals and 16 representative I-x (N2F20) mice. Spleens were quickly frozen on dry
531 ice and were then stored at -80°C until DNA was extracted using the Gentra Puregene
532 Mouse Tail/Tissue Kit (Catalog number 158906 - Cell Lysis Solution, 158918 -
533 Puregene Proteinase K, 158922 - RNase A Solution, and 158910 - Protein Precipitation
534 Solution; Qiagen, Germantown, MD, USA) according to manufacturer instructions. DNA
535 was dissolved in sterile RNAse free H2O and concentrations were determined using a
536 NanoDrop spectrophotometer (ND-2000, ThermoFisher Scientific, Waltham, MA, USA)
537 and Qubit 2.0 fluorometric quantitation (Q32866, ThermoFisher Scientific, Waltham, MA,
538 USA). DNA samples for the 16 individuals of each of the two lines were pooled into two
539 samples that were used for whole exome sequencing.

540 Whole-exome capture, sequencing, and analysis were performed by the UT
541 Southwestern McDermott Center Next-Generation Sequencing and Bioinformatics Core.
542 After initial DNA quality assessment on a 1.8% agarose gel and concentration
543 quantification using a Qubit 3.0 Fluorometer (Invitrogen, Carlsbad, CA USA), fragment
544 libraries were prepared using SureSelectXT2 HSQ Reagent Kit (Agilent Technologies,
545 Inc., Santa Clara, CA, USA). Samples were sheared on the Covaris S-2 sonicator
546 (Covaris, Woburn, MA, USA) and end-repaired, after which the 3' ends were adenylated
547 and barcoded with pre-capture indexing adapters. Following amplification and

548 purification, the sizes of the fragment libraries were assessed on the Agilent 2100
549 BioAnalyzer (Agilent Technologies, Inc., Santa Clara, CA, USA) and concentrations
550 were once again determined by Qubit fluorometric quantitation. Samples were pooled in
551 equimolar amounts and captured with the SureSelectXT2 Target Enrichment System for
552 Mouse (Agilent Technologies, Inc., Santa Clara, CA, USA), followed by a final Qubit
553 concentration quantification, and were run on the Illumina NextSeq 500 platform
554 (Illumina Inc., San Diego, CA, USA) using 150PE SBS v2 chemistry. Sequence reads
555 were mapped to the Genome Reference Consortium GRCm38 reference genomic
556 sequence for C57BL/6J using BWA (Li and Durbin, 2009). Both samples resulted in
557 mean coverage greater than 120X. Variants were called using the Genome Analysis
558 ToolKit (GATK) (McKenna et al., 2010), and annotated using snpEff (Cingolani et al.,
559 2012). Reads were visualized and plotted using the Broad Institute Integrative
560 Genomics Viewer (IGV) to detect homozygous mutations present in both samples.
561
562 Genotyping
563 NaOH-extracted DNA from tailtip samples taken at weaning from progeny of selected
564 crosses was genotyped for the presence of the *twiggy* mutation with real-time PCR to
565 detect the SNP using the following primers: Slc2a4 Forward (ccagagaccacctacatggc)
566 Slc2a4 WTReverse (GTCGGCATGGGTTTCCAGaAT) and Slc2a4 MutantReverse
567 (GTCGGCATGGGTTTCCAGaAa). PCR reactions were done in a 10 μl volume using
568 ~10 ng genomic DNA template with KAPA SYBR Fast ABI Prism 2X qPCR Master Mix
569 (KK4617; KAPA Biosystems, Wilmington, MA, USA), on an ABI 7900HT Fast Real-Time

570 PCR Machine (Applied Biosystem, Inc., Foster City, CA, USA) using MicroAmp 384-well
571 Optical Reaction Plates (Applied Biosystems, Inc., Foster City, CA, USA) with the
572 following thermo-cycling conditions: 95°C for 3 min followed by 40 cycles of 95°C for 3
573 sec and 62°C for 20 sec.
574
575 Glucose Tolerance Test
576 Progeny of select crosses were fasted for 4h during the middle of the light phase (a time
577 when mice do not normally eat). Body weights were measured at the beginning and the
578 end of the 4h fast, and initial blood glucose was determined from a small droplet of
579 blood taken from the tip of the tail using the Precision Xtra blood glucose meters and
580 glucose test strips (Abbott Diabetes Care Inc., Almeda, CA, USA). Mice were then given
581 an I.P. injection of 10% sterile glucose solution (1 g/kg; Sigma-Aldrich, St. Louis, MO,
582 USA), and blood glucose values were measured again at 15, 30, 45, 60 and 120 min
583 post injection.
584
585 Endurance Treadmill Test
586 To test exercise endurance capacity, mice of both sexes from selected crosses were
587 run on a progressive treadmill running protocol. The mice were acclimatized to the
588 motorized treadmill (Animal Treadmill Exer-3/6, Columbus Instruments, Columbus, OH,
589 USA) for two days prior to the endurance test. Day 1 of acclimatization lasted 20 min
590 consisting of 5 min on the treadmill at rest (0 m/min), 5 min at 8 m/min, 5 min at 10
591 m/min, followed by 5 min of rest (0 m/min). Day 2 also lasted 20 min and consisted of 5

592 min on the treadmill at rest (0 m/min), 5 min at 10 m/min, 5 min at 12 m/min, followed by
593 5 min of rest (0 m/min). On day 3, mice performed the endurance test to exhaustion,
594 defined as when the mouse spent more than 5 sec on the shock grid (0.1 mA x163 V
595 and 1 Hz) without re-engaging with the treadmill, as described previously (Fujikawa et
596 al., 2016). The mice ran at a speed of 10 m/min for the first 40 min, then the rate was
597 increased at 1 m/min every 10 min until the speed reached 13 m/min, at which point the
598 speed was increased at a rate of 1 m/min every 5 min until exhaustion. Mice were then
599 removed from the treadmill and blood glucose and lactate were immediately measured
600 from tail blood using hand-held analyzers for glucose (Bayer Contour Blood Glucose
601 Meter, Ascensia Diabetes Care US, Inc., Parsippany, NJ, USA) and lactate (Nova
602 Biomedical Lactate Plus Meter, Waltham, MA, USA). Mice were euthanized by
603 decapitation, and muscles were rapidly dissected and frozen on dry ice. All tissues were
604 stored at -80°C until used.
605
606 Western Blotting
607 Frozen gastrocnemius muscles collected from mice following the treadmill study were
608 homogenized in ice-cold lysis buffer composed of T-PER® buffer (#78510,
609 ThermoFisher Scientific, Waltham, MA, USA), 1% (v/v) of protease inhibitors cocktail
610 (P8340-5ML, Sigma-Aldrich, St. Louis, MO, USA), and phosphatase inhibitors cocktail 2
611 and 3 (P5726-5ML and P0044-5ML, Sigma-Aldrich, St. Louis, MO, USA). Samples were
612 homogenized using TissueLyser II homogenizer (Qiagen Inc., Valencia, CA, USA).
613 Homogenates were then solubilized by constant rotation for 1h at 4°C, and 10 min x

614 1,000 *g* at 4°C. Protein concentration of the supernatant was determined via the Pierce
615 BCA protein assay kit (#23225, ThermoFisher Scientific, Waltham, MA, USA). Samples
616 were then stored at -80°C until further analysis. Equal amounts of total protein (20 μg)
617 per sample were diluted with appropriate volume of laemmle sample buffer (2X
618 concentrated; 4% SDS, 10% 2-mercaptoethanol, 20% glycerol, 0.004% bromophenol
619 blue and 0.125 M pH6.8 Tris-HCl), heated for 5 min at 95°C, separated via SDS-PAGE,
620 and transferred to nitrocellulose (Trans-blot turbo, Bio-Rad, Hercules, CA, USA).
621 Membranes were incubated with the appropriate primary (GLUT4 #2213 and β-Actin
622 #3700, Cell Signaling Technologies, Danvers, MA, USA) and fluorescent secondary
623 antibodies (IRDye 680 Goat anti-Mouse IgG, Li-Cor Bioscience, Lincoln, NE, USA).
624 Protein band fluorescence was quantified via Li-Cor Odessy Image studio Version 4.0
625 (Li-Cor Bioscience, Lincoln, NE, USA). Individual values are relative to the mean of all
626 sample values within the same membrane, and equal loading was confirmed and
627 normalized to the immuno-reactivity of β-Actin.
628
629 Data Analysis and Statistics
630 All data were analyzed and data plots were generated using Prism 6 (GraphPad
631 Software, Inc., La Jolla, CA, USA). Statistical comparisons were made using ANOVA
632 with post hoc analyses to compare groups. Tests with $p < 0.05$ were deemed
633 statistically significant. Unless otherwise stated, all values plotted are presented as
634 mean ± SD, with statistical results presented as * = $p < 0.05$, ** = $p < 0.01$, *** = $p <$
635 0.001 and **** = $p < 0.0001$.

AUTHOR CONTRIBUTIONS

Experiments were designed by MHMdG, CMC, VK, JAM, and JST. Animal care and line maintenance was done by MHMdG. MHMdG, CMC, VK, JAM, and NIA performed the experiments and collected the data. Data analysis, interpretation and the generation of figures was done by MHMdG, CMC, VK, JAM and JST. The manuscript was written, reviewed and edited by MHMdG, CMC, VK, JAM and JST. JST directed and funded the research.

ACKNOWLEDGMENTS

Research was supported by the NIH (#U01 MH 61915) and the Howard Hughes Medical Institute (JST). Additional funding was received by CMC from the NIDDK (F32DK104659). We would like to thank Delali Bassowou, Kelly Bruckmann, Kelly Foster, Kyung-Inn Kim, Izabela Kornblum, Sammie McMurray, Chris Olker, and Dawn Olson for technical assistance. We thank Sandy Siepka and Martha Vitaterna for production of the ENU mutagenized mice and design of the initial phenotypic screen. JST is a co-founder of, a Scientific Advisory Board member of, and a paid consultant for Reset Therapeutics, Inc., a biotechnology company aimed at discovering small-molecule therapies that modulate circadian activity for a variety of disease indications. JST is an Investigator, and MHMdG. is a Research Specialist, in the Howard Hughes Medical Institute.

REFERENCES

Alvim RO, MR Cheuhen, SR Machado, AG Sousa and PC Santos. 2015. General aspects of muscle glucose uptake. *An Acad Bras Cienc* **87**: 351-368. doi: https://doi.org/10.1590/0001-3765201520140225.

Anisman H, J Gibb and S Hayley. 2008. Influence of continuous infusion of interleukin-1beta on depression-related processes in mice: corticosterone, circulating cytokines, brain monoamines, and cytokine mRNA expression. *Psychopharmacology (Berl)* **199**: 231-244. doi: https://doi.org/10.1007/s00213-008-1166-z.

Ashrafi G, Z Wu, RJ Farrell and TA Ryan. 2017. GLUT4 Mobilization Supports Energetic Demands of Active Synapses. *Neuron* **93**: 606-615 e603. doi: https://doi.org/10.1016/j.neuron.2016.12.020.

Bonsall DR, H Kim, C Tocci, A Ndiaye, A Petronzio, G McKay-Corkum, et al. 2015. Suppression of Locomotor Activity in Female C57Bl/6J Mice Treated with Interleukin-1beta: Investigating a Method for the Study of Fatigue in Laboratory Animals. *PLoS One* **10**: e0140678. doi: https://doi.org/10.1371/journal.pone.0140678.

Broman KW, H Wu, S Sen and GA Churchill. 2003. R/qtl: QTL mapping in experimental crosses. *Bioinformatics* **19**: 889-890. doi: https://doi.org/10.1093/bioinformatics/btg112.

Charron MJ, FC Brosius, SL Alper and HF Lodish. 1989. A glucose transport protein expressed predominately in insulin-responsive tissues. *Proc Natl Acad Sci USA* **86**: 2535-2539. doi: https://doi.org/10.1073/pnas.86.8.2535.

Choeiri C, W Staines and C Messier. 2002. Immunohistochemical localization and quantification of glucose transporters in the mouse brain. *Neuroscience* **111**: 19-34. doi: https://doi.org/10.1016/s0306-4522(01)00619-4.

Cingolani P, A Platts, L Wang le, M Coon, T Nguyen, L Wang, et al. 2012. A program for annotating and predicting the effects of single nucleotide polymorphisms, SnpEff: SNPs in the genome of Drosophila melanogaster strain w1118; iso-2; iso-3. *Fly (Austin)* **6**: 80-92. doi: https://doi.org/10.4161/fly.19695.

Clark AT, D Goldowitz, JS Takahashi, MH Vitaterna, SM Siepka, LL Peters, et al. 2004. Implementing large-scale ENU mutagenesis screens in North America. *Genetica* **122**: 51-64. doi: https://doi.org/10.1007/978-1-4020-5057-2_6.

Collado-Hidalgo A, JE Bower, PA Ganz, MR Irwin and SW Cole. 2008. Cytokine gene polymorphisms and fatigue in breast cancer survivors: early findings. *Brain Behav Immun* **22**: 1197-1200. doi: https://doi.org/10.1016/j.bbi.2008.05.009.

Cordes SP. 2005. N-ethyl-N-nitrosourea mutagenesis: boarding the mouse mutant express. *Microbiol Mol Biol Rev* **69**: 426-439. doi: https://doi.org/10.1128/MMBR.69.3.426-439.2005.

Dawes M, T Moore-Harrison, AT Hamilton, T Ceaser, KJ Kochan, PK Riggs, et al. 2014. Differential gene expression in high- and low-active inbred mice. *Biomed Res Int* **2014**: 361048. doi: https://doi.org/10.1155/2014/361048.

Fam BC, LJ Rose, R Sgambellone, Z Ruan, J Proietto and S Andrikopoulos. 2012. Normal muscle glucose uptake in mice deficient in muscle GLUT4. *J Endocrinol* **214**: 313-327. doi: https://doi.org/10.1530/JOE-12-0032.

Fan W and RM Evans. 2017. Exercise Mimetics: Impact on Health and Performance. *Cell Metab* **25**: 242-247. doi: https://doi.org/10.1016/j.cmet.2016.10.022.

Fan W, W Waizenegger, CS Lin, V Sorrentino, MX He, CE Wall, et al. 2017. PPARdelta Promotes Running Endurance by Preserving Glucose. *Cell Metab* **25**: 1186-1193 e1184. doi: https://doi.org/10.1016/j.cmet.2017.04.006.

Fritschi C and L Quinn. 2010. Fatigue in patients with diabetes: a review. *J Psychosom Res* **69**: 33-41. doi: https://doi.org/10.1016/j.jpsychores.2010.01.021.

Fueger PT, CY Li, JE Ayala, J Shearer, DP Bracy, MJ Charron, et al. 2007. Glucose kinetics and exercise tolerance in mice lacking the GLUT4 glucose transporter. *J Physiol* **582**: 801-812. doi: https://doi.org/10.1113/jphysiol.2007.132902.

Fujikawa T, CM Castorena, M Pearson, CM Kusminski, N Ahmed, PK Battiprolu, et al. 2016. SF-1 expression in the hypothalamus is required for beneficial metabolic effects of exercise. *Elife* **5**. doi: https://doi.org/10.7554/eLife.18206.

Fukuda K, SE Straus, I Hickie, MC Sharpe, JG Dobbins, A Komaroff, et al. 1994. The chronic fatigue syndrome: A comprehensive approach to its defintion and study. *Ann Intern Med* **121**: 953-959. doi: https://doi.org/10.7326/0003-4819-121-12-199412150-00009.

Gannon NP, CA Conn and RA Vaughan. 2015. Dietary stimulators of GLUT4 expression and translocation in skeletal muscle: a mini-review. *Mol Nutr Food Res* **59**: 48-64. doi: https://doi.org/10.1002/mnfr.201400414.

Germain A, D Ruppert, SM Levine and MR Hanson. 2017. Metabolic profiling of a myalgic encephalomyelitis/chronic fatigue syndrome discovery cohort reveals disturbances in fatty acid and lipid metabolism. *Mol Biosyst* **13**: 371-379. doi: https://doi.org/10.1039/c6mb00600k.

Goldowitz D, WN Frankel, JS Takahashi, M Holtz-Vitaterna, C Bult, WA Kibbe, et al. 2004. Large-scale mutagenesis of the mouse to understand the genetic bases of nervous system structure and function. *Brain Res Mol Brain Res* **132**: 105-115. doi: https://doi.org/10.1016/j.molbrainres.2004.09.016.

Golumbek PT, RM Keeling and AM Connolly. 2007. RAG2 gene knockout in mice causes fatigue. *Muscle Nerve* **36**: 471-476. doi: https://doi.org/10.1002/mus.20834.

Gorselink M, MR Drost, KF de Brouwer, G Schaart, GP van Kranenburg, TH Roemen, et al. 2002. Increased muscle fatigability in GLUT-4-deficient mice. *Am J Physiol Endocrinol Metab* **282**: E348-354. doi: https://doi.org/10.1152/ajpendo.00085.2001.

Govers R. 2014. Cellular regulation of glucose uptake by glucose transporter GLUT4. *Adv Clin Chem* **66**: 173-240. doi: https://doi.org/10.1016/b978-0-12-801401-1.00006-2.

Hardy SE and SA Studenski. 2008a. Fatigue and function over three years among older adults. *J Gerontol A Biol Sci Med Sci* **63**: 1389-1392. doi: https://doi.org/10.1093/gerona/63.12.1389.

Hardy SE and SA Studenski. 2008b. Fatigue predicts mortality in older adults. *J Am Geriatr Soc* **56**: 1910-1914. doi: https://doi.org/10.1111/j.1532-5415.2008.01957.x.

Harno E, EC Cottrell and A White. 2013. Metabolic pitfalls of CNS Cre-based technology. *Cell Metab* **18**: 21-28. doi: https://doi.org/10.1016/j.cmet.2013.05.019.

Harrington ME. 2012. Neurobiological studies of fatigue. *Prog Neurobiol* **99**: 93-105. doi: https://doi.org/10.1016/j.pneurobio.2012.07.004.

Huang S and MP Czech. 2007. The GLUT4 glucose transporter. *Cell Metab* **5**: 237-252. doi: https://doi.org/10.1016/j.cmet.2007.03.006.

Jason LA, M Evans, M Brown and N Porter. 2010. What is fatigue? Pathological and nonpathological fatigue. *PM R* **2**: 327-331. doi: https://doi.org/10.1016/j.pmrj.2010.03.028.

Jiang H, J Li, EB Katz and MJ Charron. 2001. GLUT4 ablation in mice results in redistribution of IRAP to the plasma membrane. *Biochem Biophys Res Commun* **284**: 519-525. doi: https://doi.org/10.1006/bbrc.2001.4994.

Johnston S, D Staines, A Klein and S Marshall-Gradisnik. 2016. A targeted genome association study examining transient receptor potential ion channels, acetylcholine receptors, and adrenergic receptors in Chronic Fatigue Syndrome/Myalgic Encephalomyelitis. *BMC Med Genet* **17**: 79. doi: https://doi.org/10.1186/s12881-016-0342-y.

Jordan SD, A Kriebs, M Vaughan, D Duglan, W Fan, E Henriksson, et al. 2017. CRY1/2 Selectively Repress PPARdelta and Limit Exercise Capacity. *Cell Metab* **26**: 243-255 e246. doi: https://doi.org/10.1016/j.cmet.2017.06.002.

Justice MJ, JK Noveroske, JS Weber, B Zheng and A Bradley. 1999. Mouse ENU Mutagenesis. *Human Mol Genetics* **8**: 1955-1963. doi: https://doi.org/10.1093/hmg/8.10.1955.

Katz EB, AE Stenbit, K Hatton, R DePinho and MJ Charron. 1995. Cardiac and adipose tissue abnormalities but not diabetes in mice deficient in GLUT4. *Nature* **377**: 151-155. doi: https://doi.org/10.1038/377151a0.

Keays DA and PM Nolan. 2003. N-ethyl-N-nitrosourea mouse mutants in the dissection of behavioural and psychiatric disorders. *European Journal of Pharmacology* **480**: 205-217. doi: https://doi.org/10.1016/j.ejphar.2003.08.107.

Klimas NG, G Broderick and MA Fletcher. 2012. Biomarkers for chronic fatigue. *Brain Behav Immun* **26**: 1202-1210. doi: https://doi.org/10.1016/j.bbi.2012.06.006.

Krzyszton CP, NL Sparkman, RW Grant, JB Buchanan, SR Broussard, J Woods, et al. 2008. Exacerbated fatigue and motor deficits in interleukin-10-deficient mice after peripheral immune stimulation. *Am J Physiol Regul Integr Comp Physiol* **295**: R1109-1114. doi: https://doi.org/10.1152/ajpregu.90302.2008.

Kudo T, DH Loh, D Truong, Y Wu and CS Colwell. 2011a. Circadian dysfunction in a mouse model of Parkinson's disease. *Exp Neurol* **232**: 66-75. doi: https://doi.org/10.1016/j.expneurol.2011.08.003.

Kudo T, A Schroeder, DH Loh, D Kuljis, MC Jordan, KP Roos, et al. 2011b. Dysfunctions in circadian behavior and physiology in mouse models of Huntington's disease. *Exp Neurol* **228**: 80-90. doi: https://doi.org/10.1016/j.expneurol.2010.12.011.

Kumar V, K Kim, C Joseph, LC Thomas, H Hong and JS Takahashi. 2011. Second-generation high-throughput forward genetic screen in mice to isolate subtle behavioral mutants. *Proc Natl Acad Sci U S A* **108**: 15557-15564. doi: https://doi.org/10.1073/pnas.1107726108.

Kumar V, K Kim, C Joseph, S Kourrich, SH Yoo, HC Huang, et al. 2013. C57BL/6N mutation in cytoplasmic FMRP interacting protein 2 regulates cocaine response. *Science* **342**: 1508-1512. doi: https://doi.org/10.1126/science.1245503.

Landmark-Hoyvik H, KV Reinertsen, JH Loge, VN Kristensen, V Dumeaux, SD Fossa, et al. 2010. The genetics and epigenetics of fatigue. *PM R* **2**: 456-465. doi: https://doi.org/10.1016/j.pmrj.2010.04.003.

Lasselin J, S Laye, JB Barreau, A Rivet, MJ Dulucq, H Gin, et al. 2012. Fatigue and cognitive symptoms in patients with diabetes: relationship with disease phenotype and insulin treatment. *Psychoneuroendocrinology* **37**: 1468-1478. doi: https://doi.org/10.1016/j.psyneuen.2012.01.016.

Li H and R Durbin. 2009. Fast and accurate short read alignment with Burrows-Wheeler transform. *Bioinformatics* **25**: 1754-1760. doi: https://doi.org/10.1093/bioinformatics/btp324.

Li J, KL Houseknecht, AE Stenbit, EB Katz and MJ Charron. 2000. Reduced glucose uptake precedes insulin signaling defects in adipocytes from heterozygous GLUT4 knockout mice. *FASEB J* **14**: 1117-1125.

Lightfoot JT. 2011. Current understanding of the genetic basis for physical activity. *J Nutr* **141**: 526-530. doi: https://doi.org/10.3945/jn.110.127290.

Lin E and LC Huang. 2008. Identification of significant genes in genomics using Bayesian variable selection methods. *Adv Appl Bioinform Chem* **1**: 13-18. doi: https://doi.org/10.2147/aabc.s3624.

Lin HV, H Ren, VT Samuel, HY Lee, TY Lu, GI Shulman, et al. 2011. Diabetes in mice with selective impairment of insulin action in Glut4-expressing tissues. *Diabetes* **60**: 700-709. doi: https://doi.org/10.2337/db10-1056.

Liu ML, AL Olson, WS Moye-Rowley, JB Buse, GI Bell and JE Pessin. 1992. Expression and regulation of the human GLUT4/muscle-fat facilitative glucose transporter gene in transgenic mice. *J Biol Chem* **267**: 11673-11676.

Maes M and FNM Twisk. 2010. Chronic fatigue syndrome: Harvey and Wessely's (bio)psychosocial model versus a bio(psychosocial) model based on inflammatory and oxidative and nitrosative stress pathways. *BMC Medicine* **8**: 1-13. doi: https://doi.org/10.1186/1741-7015-8-35.

Maxmen A. 2017. Biological underpinnings of chronic fatigue syndrome begin to emerge. *Nature* **543**: 602. doi: https://doi.org/10.1038/543602a.

McKenna A, M Hanna, E Banks, A Sivachenko, K Cibulskis, A Kernytsky, et al. 2010. The Genome Analysis Toolkit: a MapReduce framework for analyzing next-generation DNA sequencing data. *Genome Res* **20**: 1297-1303. doi: https://doi.org/10.1101/gr.107524.110.

Moreh E, JM Jacobs and J Stessman. 2010. Fatigue, function, and mortality in older adults. *J Gerontol A Biol Sci Med Sci* **65**: 887-895. doi: https://doi.org/10.1093/gerona/glq064.

Moresco EM, X Li and B Beutler. 2013. Going forward with genetics: recent technological advances and forward genetics in mice. *Am J Pathol* **182**: 1462-1473. doi: https://doi.org/10.1016/j.ajpath.2013.02.002.

Morris G, M Berk, K Walder and M Maes. 2015. The Putative Role of Viruses, Bacteria, and Chronic Fungal Biotoxin Exposure in the Genesis of Intractable Fatigue Accompanied by Cognitive and Physical Disability. *Mol Neurobiol* **53**: 2550-2571. doi: https://doi.org/10.1007/s12035-015-9262-7.

Moulton CD, JC Pickup and K Ismail. 2015. The link between depression and diabetes: the search for shared mechanisms. *Lancet Diabetes Endocrinol* **3**: 461-471. doi: https://doi.org/10.1016/S2213-8587(15)00134-5.

Nakamura TJ, W Nakamura, S Yamazaki, T Kudo, T Cutler, CS Colwell, et al. 2011. Age-related decline in circadian output. *J Neurosci* **31**: 10201-10205. doi: https://doi.org/10.1523/JNEUROSCI.0451-11.2011.

Narita M, N Nishigami, N Narita, K Yamaguti, N Okado, Y Watanabe, et al. 2003. Association between serotonin transporter gene polymorphism and chronic fatigue syndrome. *Biochem Biophys Res Commun* **311**: 264-266. doi: https://doi.org/10.1016/j.bbrc.2003.09.207.

Narkar VA, M Downes, RT Yu, E Embler, YX Wang, E Banayo, et al. 2008. AMPK and PPARdelta agonists are exercise mimetics. *Cell* **134**: 405-415. doi: https://doi.org/10.1016/j.cell.2008.06.051.

Ottenweller JE, BH Natelson, WC Gause, KK Carroll, D Beldowicz, XD Zhou, et al. 1998. Mouse Running Activity Is Lowered by Brucella abortus Treatment: A

Potential Model to Study Chronic Fatigue. *Physiol Behav* **63**: 795-801. doi: https://doi.org/10.1016/s0031-9384(97)00539-8.

Pack AI, RJ Galante, G Maislin, J Cater, D Metaxas, S Lu, et al. 2007. Novel method for high-throughput phenotyping of sleep in mice. *Physiol Genomics* **28**: 232-238. doi: https://doi.org/10.1152/physiolgenomics.00139.2006.

Petersen HH, TK Andreassen, T Breiderhoff, JH Brasen, H Schulz, V Gross, et al. 2006. Hyporesponsiveness to glucocorticoids in mice genetically deficient for the corticosteroid binding globulin. *Mol Cell Biol* **26**: 7236-7245. doi: https://doi.org/10.1128/MCB.00400-06.

Ranjith G. 2005. Epidemiology of chronic fatigue syndrome. *Occup Med (Lond)* **55**: 13-19. doi: https://doi.org/10.1093/occmed/kqi012.

Ray MA, RA Trammell, S Verhulst, S Ran and LA Toth. 2011. Development of a Mouse Model for Assessing Fatigue during Chemotherapy. *Comp Medicine* **61**: 119-130.

Ren H, S Yan, B Zhang, TY Lu, O Arancio and D Accili. 2014. Glut4 expression defines an insulin-sensitive hypothalamic neuronal population. *Mol Metab* **3**: 452-459. doi: https://doi.org/10.1016/j.molmet.2014.04.006.

Ren H, TY Lu, TE McGraw and D Accili. 2015. Anorexia and Impaired Glucose Metabolism in Mice With Hypothalamic Ablation of Glut4 Neurons. *Diabetes* **64**: 405-417. doi: https://doi.org/10.2337/db14-0752/-/DC1.

Reno CM, EC Puente, Z Sheng, D Daphna-Iken, AJ Bree, VH Routh, et al. 2017. Brain GLUT4 Knockout Mice Have Impaired Glucose Tolerance, Decreased Insulin Sensitivity, and Impaired Hypoglycemic Counterregulation. *Diabetes* **66**: 587-597. doi: https://doi.org/10.2337/db16-0917.

Rossetti L, AE Stenbit, W Chen, M Hu, N Barzilai, EB Katz, et al. 1997. Peripheral but not hepatic insulin resistance in mice with one disrupted allele of the glucose

transporter type 4 (GLUT4) gene. *J Clin Invest* **100**: 1831-1839. doi: https://doi.org/10.1172/JCI119711.

Sadler JB, NJ Bryant, GW Gould and CR Welburn. 2013. Posttranslational modifications of GLUT4 affect its subcellular localization and translocation. *Int J Mol Sci* **14**: 9963-9978. doi: https://doi.org/10.3390/ijms14059963.

Saligan LN, K Olson, K Filler, D Larkin, F Cramp, S Yennurajalingam, et al. 2015. The biology of cancer-related fatigue: a review of the literature. *Support Care Cancer* **23**: 2461-2478. doi: https://doi.org/10.1007/s00520-015-2763-0.

Schlauch KA, SF Khaiboullina, KL De Meirleir, S Rawat, J Petereit, AA Rizvanov, et al. 2016. Genome-wide association analysis identifies genetic variations in subjects with myalgic encephalomyelitis/chronic fatigue syndrome. *Transl Psychiatry* **6**: e730. doi: https://doi.org/10.1038/tp.2015.208.

Schur E, N Afari, J Goldberg, D Buchwald and PF Sullivan. 2007. Twin analyses of fatigue. *Twin Res Hum Genet* **10**: 729-733. doi: https://doi.org/10.1375/twin.10.5.729.

Shimomura K, SS Low-Zeddies, DP King, TD Steeves, A Whiteley, J Kushla, et al. 2001. Genome-wide epistatic interaction analysis reveals complex genetic determinants of circadian behavior in mice. *Genome Res* **11**: 959-980. doi: https://doi.org/10.1101/gr.171601.

Siepka SM and JS Takahashi. 2005a. Forward genetic screens to identify circadian rhythm mutants in mice. *Methods Enzymol* **393**: 219-229. doi: https://doi.org/10.1016/S0076-6879(05)93007-3.

Siepka SM and JS Takahashi. 2005b. Methods to record circadian rhythm wheel running activity in mice. *Methods Enzymol* **393**: 230-239. doi: https://doi.org/10.1016/S0076-6879(05)93008-5.

Simoes MV, S Egert, S Ziegler, M Miyagawa, S Reder, T Lehner, et al. 2004. Delayed response of insulin-stimulated fluorine-18 deoxyglucose uptake in glucose transporter-4-null mice hearts. *J Am Coll Cardiol* **43**: 1690-1697. doi: https://doi.org/10.1016/j.jacc.2003.12.038.

Skoie IM, T Ternowitz, G Jonsson, K Norheim and R Omdal. 2015. Fatigue in psoriasis: a phenomenon to be explored. *Br J Dermatol* **172**: 1196-1203. doi: https://doi.org/10.1111/bjd.13647.

Smith AK, I Dimulescu, VR Falkenberg, S Narasimhan, C Heim, SD Vernon, et al. 2008. Genetic evaluation of the serotonergic system in chronic fatigue syndrome. *Psychoneuroendocrinology* **33**: 188-197. doi: https://doi.org/10.1016/j.psyneuen.2007.11.001.

Smith AK, H Fang, T Whistler, ER Unger and MS Rajeevan. 2011. Convergent genomic studies identify association of GRIK2 and NPAS2 with chronic fatigue syndrome. *Neuropsychobiology* **64**: 183-194. doi: https://doi.org/10.1159/000326692.

Soewarto D, C Fella, A Teubner, B Rathkolb, W Pargent, S Heffner, et al. 2000. The large-scale Munich ENU-mouse-mutagenesis screen. *Mamm Genome* **11**: 507-510. doi: https://doi.org/10.1007/s003350010097.

Sprangers MA, MS Thong, M Bartels, A Barsevick, J Ordonana, Q Shi, et al. 2014. Biological pathways, candidate genes, and molecular markers associated with quality-of-life domains: an update. *Qual Life Res* **23**: 1997-2013. doi: https://doi.org/10.1007/s11136-014-0656-1.

Stenbit AE, TS Tsao, J Li, R Burcelin, DL Geenen, SM Factor, et al. 1997. GLUT4 heterozygous knockout mice develop muscle insulin resistance and diabetes. *Nat Med* **3**: 1096-1101. doi: https://doi.org/10.1038/nm1097-1096.

Stenbit AE, EB Katz, JC Chatham, DL Geenen, SM Factor, RG Weiss, et al. 2000. Preservation of glucose metabolism in hypertrophic GLUT4-null hearts. *Am J Physiol Heart Circ Physiol* **279**: H313-318.

Sylow L, M Kleinert, EA Richter and TE Jensen. 2017. Exercise-stimulated glucose uptake - regulation and implications for glycaemic control. *Nat Rev Endocrinol* **13**: 133-148. doi: https://doi.org/10.1038/nrendo.2016.162.

Takahashi JS, K Shimomura and V Kumar. 2008. Searching for genes underlying behavior: lessons from circadian rhythms. *Science* **322**: 909-912. doi: https://doi.org/10.1126/science.1158822.

Torpy DJ and JT Ho. 2007. Corticosteroid-binding globulin gene polymorphisms: clinical implications and links to idiopathic chronic fatigue disorders. *Clin Endocrinol (Oxf)* **67**: 161-167. doi: https://doi.org/10.1111/j.1365-2265.2007.02890.x.

Tsao TS, AE Stenbit, J Li, KL Houseknecht, JR Zierath, EB Katz, et al. 1997. Muscle-specific transgenic complementation of GLUT4-deficient mice. Effects on glucose but not lipid metabolism. *J Clin Invest* **100**: 671-677. doi: https://doi.org/10.1172/JCI119579.

Tsao TS, AE Stenbit, SM Factor, W Chen, L Rossetti and MJ Charron. 1999. Prevention of insulin resistance and diabetes in mice heterozygous for GLUT4 ablation by transgenic complementation of GLUT4 in skeletal muscle. *Diabetes* **48**: 775-782. doi: https://doi.org/10.2337/diabetes.48.4.775.

Tsao TS, J Li, KS Chang, AE Stenbit, D Galuska, JE Anderson, et al. 2001. Metabolic adaptations in skeletal muscle overexpressing GLUT4: effects on muscle and physical activity. *FASEB J* **15**: 958-969. doi: https://doi.org/10.1096/fj.00-0381.

Vitaterna MH, LH Pinto and JS Takahashi. 2006. Large-scale mutagenesis and phenotypic screens for the nervous system and behavior in mice. *Trends Neurosci* **29**: 233-240. doi: https://doi.org/10.1016/j.tins.2006.02.006.

Wang T, J Yin, AH Miller and C Xiao. 2017. A systematic review of the association between fatigue and genetic polymorphisms. *Brain Behav Immun* **62**: 230-244. doi: https://doi.org/10.1016/j.bbi.2017.01.007.

Wang YX, CL Zhang, RT Yu, HK Cho, MC Nelson, CR Bayuga-Ocampo, et al. 2004. Regulation of muscle fiber type and running endurance by PPARdelta. *PLoS Biol* **2**: e294. doi: https://doi.org/10.1371/journal.pbio.0020294.

Wessely S. 1998. The epidemiology of chronic fatigue syndrome. *Epidemiol Psichiatr Soc* **7**: 10-24.

FIGURE LEGENDS

Fig. 1. Mice from two lines show abnormal, low amplitude voluntary wheel-running activity patterns. (A) Representative actogram of a B/Int-x (N6F2) mouse showing a normal circadian activity pattern, double plotted for ease of visualization, with each horizontal line representing 48h and successive days (1-96) plotted along the Y-axis. Wheel revolutions are depicted as black marks on the horizontal lines. Mice were initially recorded under a 12h light:12h dark (LD) cycle shown in the bar across the top of the graph (black = dark phase). After 3 weeks, mice were recorded in constant darkness (DD) for 3 weeks, in 12:12 LD for 3 weeks, in constant light (LL) for 2 weeks and a final 2 weeks in DD (indicated on right Y-axis). Wheel running activity shows a normal nocturnal pattern during recording under LD with high levels of activity concentrated in the dark phase and low activity during the light phase. In DD, the rhythm free-runs with a period of ~23.7h, re-entrains normally upon reintroduction of the LD cycle, and free-runs with a lengthened period under LL. Colored vertical bars on the left side of the actogram indicate days used for quantification of wheel-running behavior. Representative actogram of a B/Int-x (N6F2) (B) and two I-x (N2F10) (C&D) mice showing an abnormal circadian activity pattern with plotting conventions and recording conditions as described for (A). (E) Representative actograms of two T-x (N3) mice recorded for 3 weeks in LD followed by 3 weeks in DD. Plotting conventions are as described for (A). (F) Average waveforms for activity recorded in LD for mice in the B/IntX (N6F2; n=40), I-x (N2F10; n=26), and T-x (N3; n=27) groups. Time (24h) is plotted along the X-axis and average number of wheel revolutions (± SEM) is plotted along the Y-axis. The LD cycle is shown in the bar across the bottom of the graph with lights off from 12 to 24 indicated in black. Average number of wheel revolutions per min over 24h (G), % of daily activity occurring in the light phase (H), and number of discreet bouts of activity occurring each day (I) during recording under LD for mice in the B/IntX (N6F2; n=40), I-x (N2F10; n=26), and T-x (N3; n=27) groups are plotted. Average number of wheel revolutions per min over 24h (J), amplitude (K) and period (L) of the wheel-running rhythm recorded in DD for these same mice is also shown. Means ± SD with individual data points are plotted in G-L with significant differences among groups indicated (* = $p < 0.05$, ** = $p < 0.01$, *** = $p < 0.001$, **** = $p < 0.0001$).

Fig. 2. Nocturnal wheel-running activity is interrupted by frequent rest bouts in affected mice. Ethogram depicting behaviors, states or locations observed in images captured once every min for 15h beginning at lights off for a wildtype C57BL/6J (A) and an I-x (N2F14) (B) mouse, with time plotted along the X-axis. Each photograph was scored on a 9 item scale using the following designations: 1) drinking, 2) eating, 3) near hopper, 4) running on wheel, 5) near wheel awake, 6) end awake, 7) end resting, 8) near wheel asleep, and 9) end asleep, where ‘end’ refers to the end of the cage furthest away from the wheel. Color code for each score is shown in the legend below (B). Pie charts

showing the amount of time spent in each of the 9 behavioral states for the first 6h of recording for the individual plotted in A (C), and averaged for all 3 wildtype C57BL/6J mice (D), the individual plotted in B (E), and averaged for all 10 I-x (N2F14/15) mice (F) are shown. Note: 5 individual I-x (N2F14/15) mice were recorded twice each with ~one week between recording days. Pictures in (G) show a representative mouse scored as "near wheel awake" (right) and "near wheel asleep" (left). See also data for individual mice plotted in Fig. S2 and S3.

Fig. 3. Video recording shows bouts of sleep during active phase in affected mice. Total number of wheel revolutions recorded for 2h to 3.5h after lights off for a T-x (N3F2) mouse and 3 individual I-x (N2F21) mice (A), and a different T-x (N3F2) and 3 individual T-x (N11F3) mice (B) are plotted, with periods of prolonged immobility consistent with sleep indicated in colored bars along the X-axis below. Periods > 40s of total immobility with low posture were scored as sleep.

Fig. 4. Abnormal phenotypes map to locus on chromosome 11. Representative actograms of an unaffected (A) and two affected (B & C) M-x (F2) mice, which were recorded for 3 weeks in LD followed by 3 weeks in DD. Plotting conventions are as those described for Fig. 1A. Average number of wheel revolutions per min recorded in LD (D) or DD (E) and amplitude of the free-running rhythm in DD (F) for mice in the WTB6B10 (F1; n=63), WTB6B10 (F2; n=112), M-x (F1; n=92) and M-x (F2; n=207) groups are shown. Genome wide linkage plots for average number of wheel revolutions per min recorded in LD (G) or DD (H) and amplitude of the free-running rhythm in DD (I) all show linkage to a locus on chromosome 11, with chromosomal location plotted along the X-axis. Average number of wheel revolutions per min recorded in LD (J), or DD (K) and amplitude of the free-running rhythm in DD (L) for mice with B6/B6 (n=26), B6/B10 (n=33), or B10/B10 (n=14) genotypes at a SNP marker (rs13481117) located on chromosome 11 at position 79252230 are plotted. Means ± SD and individual data points are plotted and significant differences among groups are indicated (* = $p < 0.05$, ** = $p < 0.01$, *** = $p < 0.001$, **** = $p < 0.0001$). See Fig. S4 for related data.

Fig. 5. Affected mice harbor a single point mutation in *Slc2a4* encoding the GLUT4 insulin-responsive glucose transporter. Results of whole-exome sequencing of spleen genomic DNA reveal a single amino acid change (A to T) at position 69944065 within the *Slc2a4* gene on chromosome 11 (A), indicated with a red arrow on the coverage plots. All reads at this locus for the I-x (N2F20) and the T-x (N11F3) samples (n=16 per group, pooled) showed this single nucleotide alteration (indicated by red line), and 19 representative reads from each sample are shown at higher magnification at the bottom of the plot. A cartoon of the GLUT4 insulin-responsive glucose transporter with its 12 trans-membrane domains is shown in (B) with the A to T SNP location and resulting

premature stop (Y440*) in exon 10 indicated with a red line. The mutation falls within the last extracellular loop and likely leads to a truncation of the cytoplasmic C-Terminus domain (indicated in grey). Protein abundance of GLUT4 in the gastrocnemius muscle of representative wildtype (+/+) and homozygous mutant (twgy/twgy) mice is shown in C with means ± SD and individual data points of +/+ or +/twgy (n=16) and twgy/twgy (n=14) plotted below. **** indicates significant difference between genotypes ($p < 0.0001$). See Fig. S5 for related data.

Fig. 6. The *twiggy* mutation of *Slc2a4* results in impaired glucose tolerance, increased heart weight, low body weight, and decreased exercise tolerance. (A) Glucose tolerance response for C57BL/6J (n=13), wildtype (+/+; n=6), heterozygous (+/twgy; n=27) and homozygous (twgy/twgy; n=56) mice. Blood glucose (mg/dL ± SEM) is plotted on the Y-axis with time since I.P. injection of glucose plotted along the X-axis. Significant differences between twgy/twgy and C57BL/6J at 15, 30 and 45 min is indicated (** = $p < 0.01$, **** = $p < 0.0001$). +/+ and +/twgy did not differ from C57BL/6J at any time point. (B) Blood glucose (mg/dL ± SD) following a 4h fast in the middle of the light phase for male (blue, left) and female (red, right) C57BL/6J (B6; n=12 M & n=5 F), +/+ (n=4 M & n=7 F), +/twgy (n=15 M & n=16 F) and twgy/twgy (n=36 M & n=3 8F) is plotted. (C) Body weights of the same mice shown in B taken after a 4h fast. Heart weights (as a percentage of total body weight) of male (blue, left) and female (red, right) C57BL/6J (B6; n=10 M & n=5 F), +/+ (n=5 M & n=8 F), +/twgy (n=18 M & n=13 F) and twgy/twgy (n=36 M & n=39 F) mice are shown in (D). A treadmill exercise test run on +/+ (n=3 M & n=3 F), +/twgy (n=16 M & n=4 F) and twgy/twgy (n=6 M & n=9 F) mice showed impaired responses in homozygous twgy/twgy mice in time (in min; E), distance (in m; F), blood glucose (G) and lactate (H) at exhaustion. Means ± SD and individual data points are plotted with significant differences indicated (* = $p < 0.05$, ** = $p < 0.01$, *** = $p < 0.001$, **** = $p < 0.0001$).

Fig. 7. *Slc2a4*$^{twgy/twgy}$ mice show abnormal, low-amplitude circadian patterns of voluntary wheel-running behavior interrupted with frequent rest bouts. (A) Representative actograms of B/Int-x (N12F2) mice of all three genotypes (+/+ - top, +/twgy - middle, twgy/twgy - bottom) recorded for 3 weeks under a full 12:12 LD cycle (shown in bar across the top). Plotting conventions are like those for Fig 1A. Colored vertical bars on the left side of the actograms indicate days used for quantification of wheel-running behavior. Average number of wheel revolutions per min over 24h (B), and % of daily activity occurring in the light phase (C) for mice in the +/+ (n=4 M & n=5 F), +/twgy (n=19 M & n=16 F), and twgy/twgy (n=41 M & n=45 F) groups are plotted. Means ± SD and individual data points are plotted with significant differences indicated (** = $p < 0.01$, *** = $p < 0.001$, **** = $p < 0.0001$).

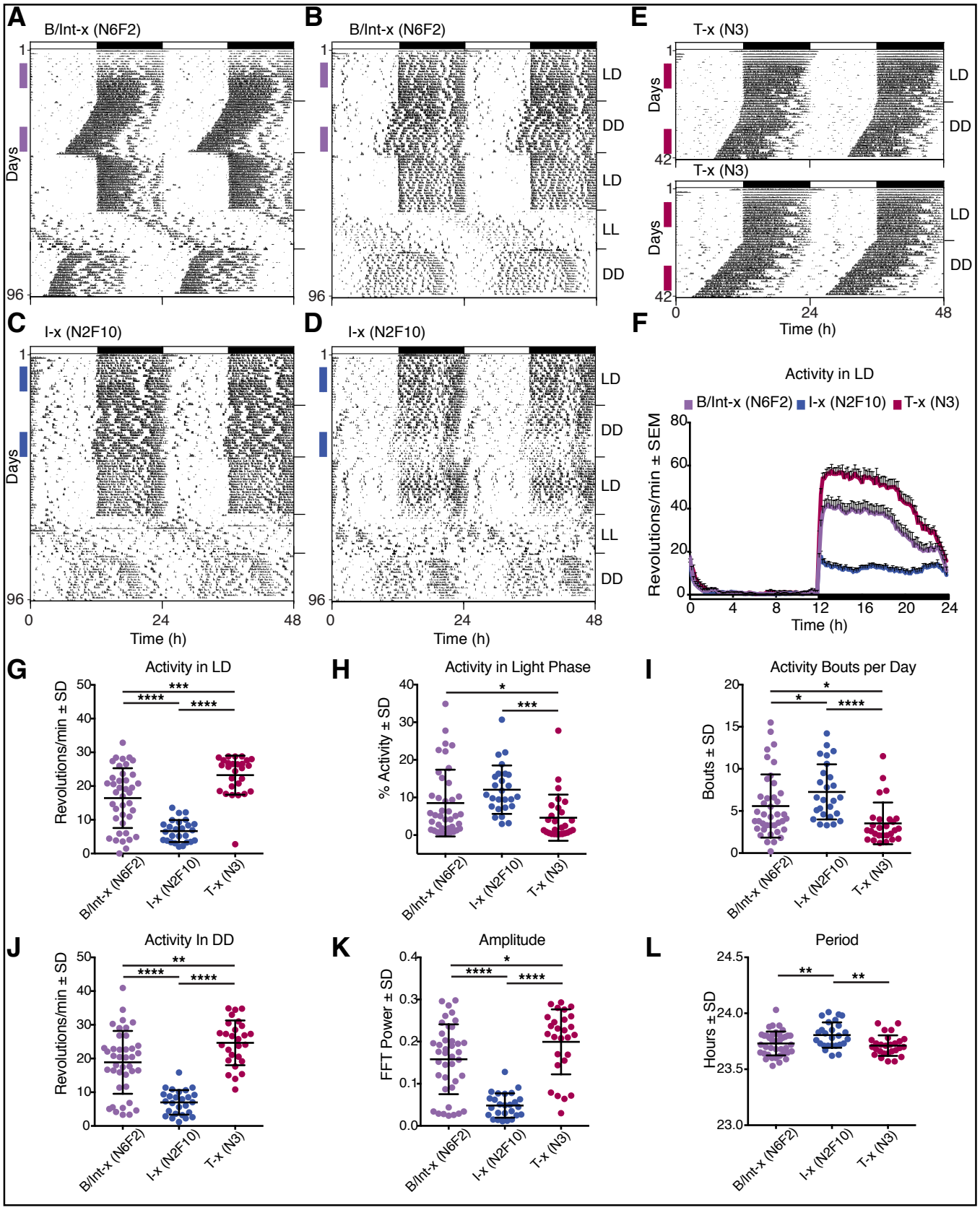
A
B/Int-x (N6F2)
B
B/Int-x (N6F2)
E
T-x (N3)
T-x (N3)
Days
LD
DD
LL
Time (h)
C
I-x (N2F10)
D
I-x (N2F10)
F
Activity in LD
B/Int-x (N6F2)
I-x (N2F10)
T-x (N3)
Revolutions/min ± SEM
G
Activity in LD
Revolutions/min ± SD
H
Activity in Light Phase
% Activity ± SD
I
Activity Bouts per Day
Bouts ± SD
J
Activity In DD
Revolutions/min ± SD
K
Amplitude
FFT Power ± SD
L
Period
Hours ± SD

Figure 1

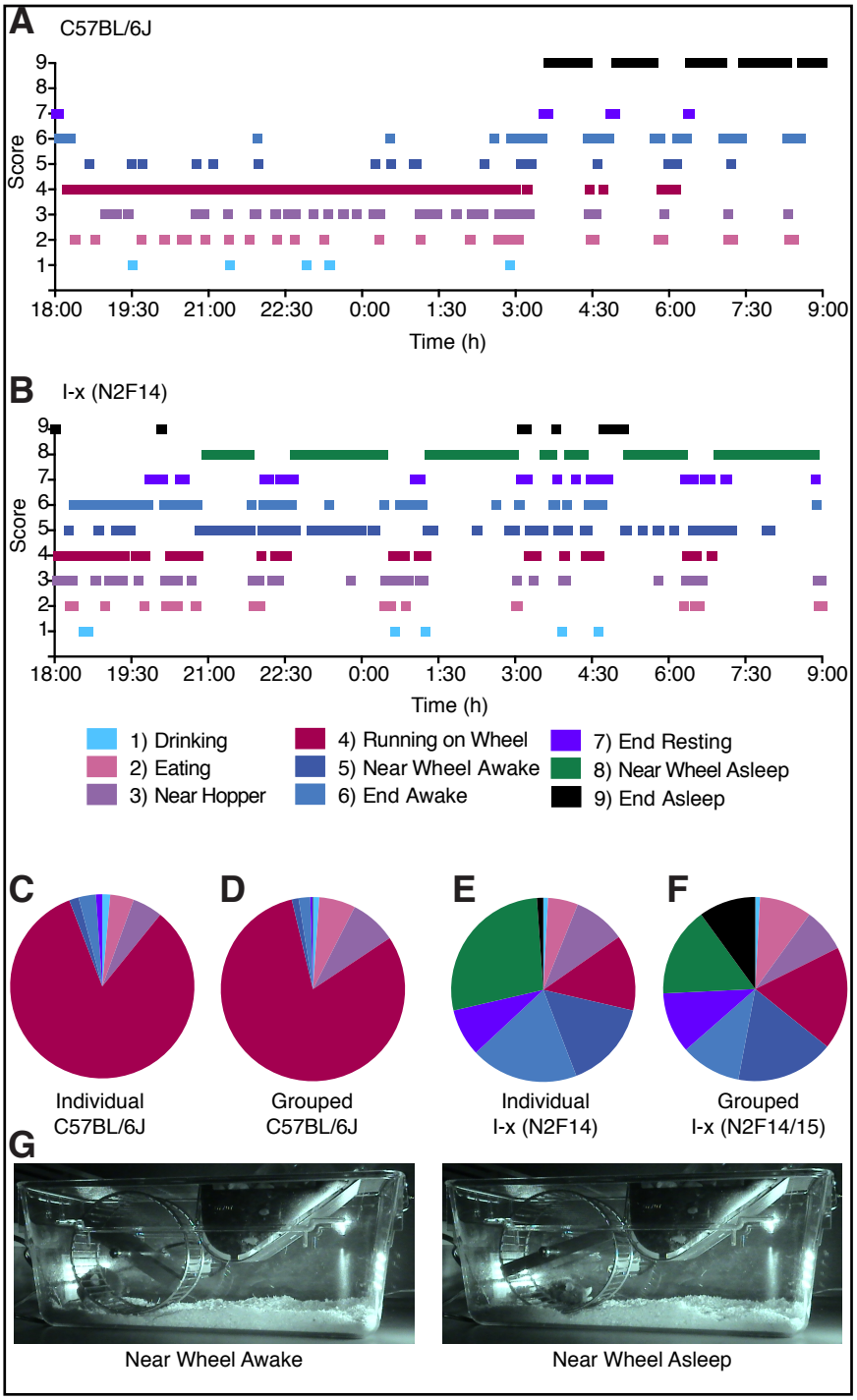
A
C57BL/6J
Score
Time (h)
18:00
19:30
21:00
22:30
0:00
1:30
3:00
4:30
6:00
7:30
9:00
B
I-x (N2F14)
1) Drinking
2) Eating
3) Near Hopper
4) Running on Wheel
5) Near Wheel Awake
6) End Awake
7) End Resting
8) Near Wheel Asleep
9) End Asleep
C
Individual C57BL/6J
D
Grouped C57BL/6J
E
Individual I-x (N2F14)
F
Grouped I-x (N2F14/15)
G
Near Wheel Awake
Near Wheel Asleep

Figure 2

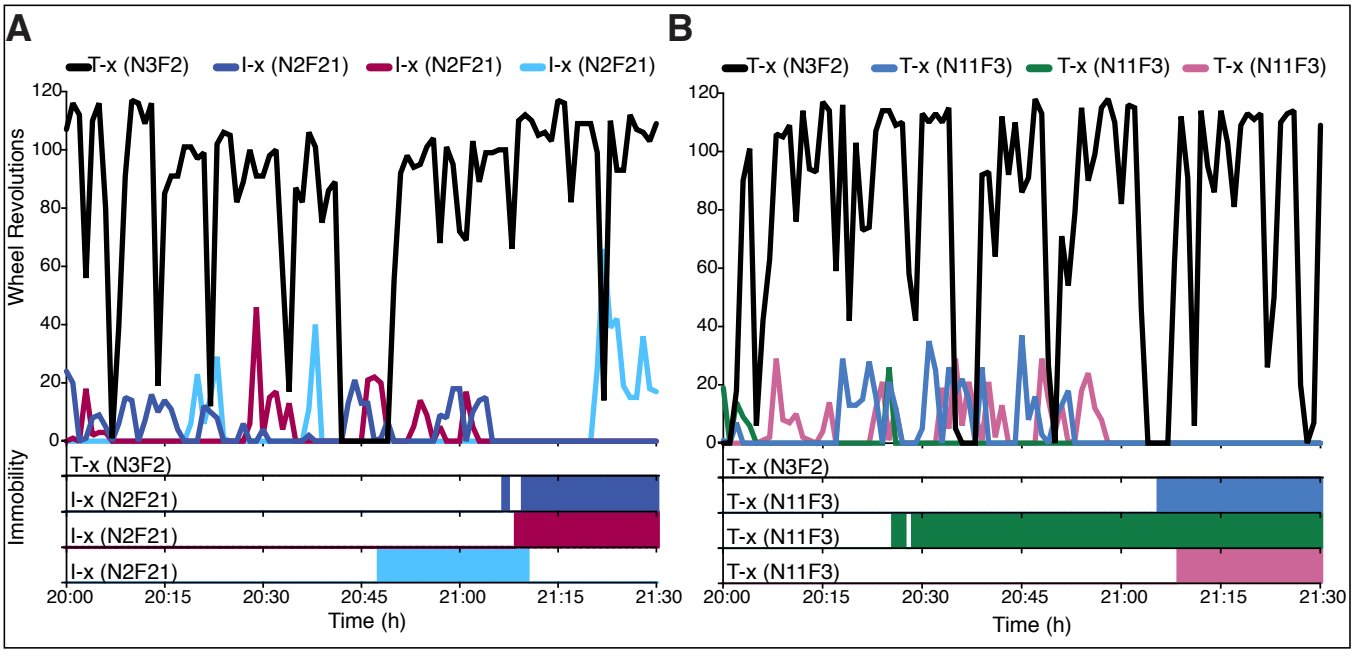
A
T-x (N3F2)
I-x (N2F21)
I-x (N2F21)
I-x (N2F21)
Wheel Revolutions
120
100
80
60
40
20
0
Immobility
T-x (N3F2)
I-x (N2F21)
I-x (N2F21)
I-x (N2F21)
20:00
20:15
20:30
20:45
21:00
21:15
21:30
Time (h)
B
T-x (N3F2)
T-x (N11F3)
T-x (N11F3)
T-x (N11F3)
120
100
80
60
40
20
0
T-x (N3F2)
T-x (N11F3)
T-x (N11F3)
T-x (N11F3)
20:00
20:15
20:30
20:45
21:00
21:15
21:30
Time (h)

Figure 3

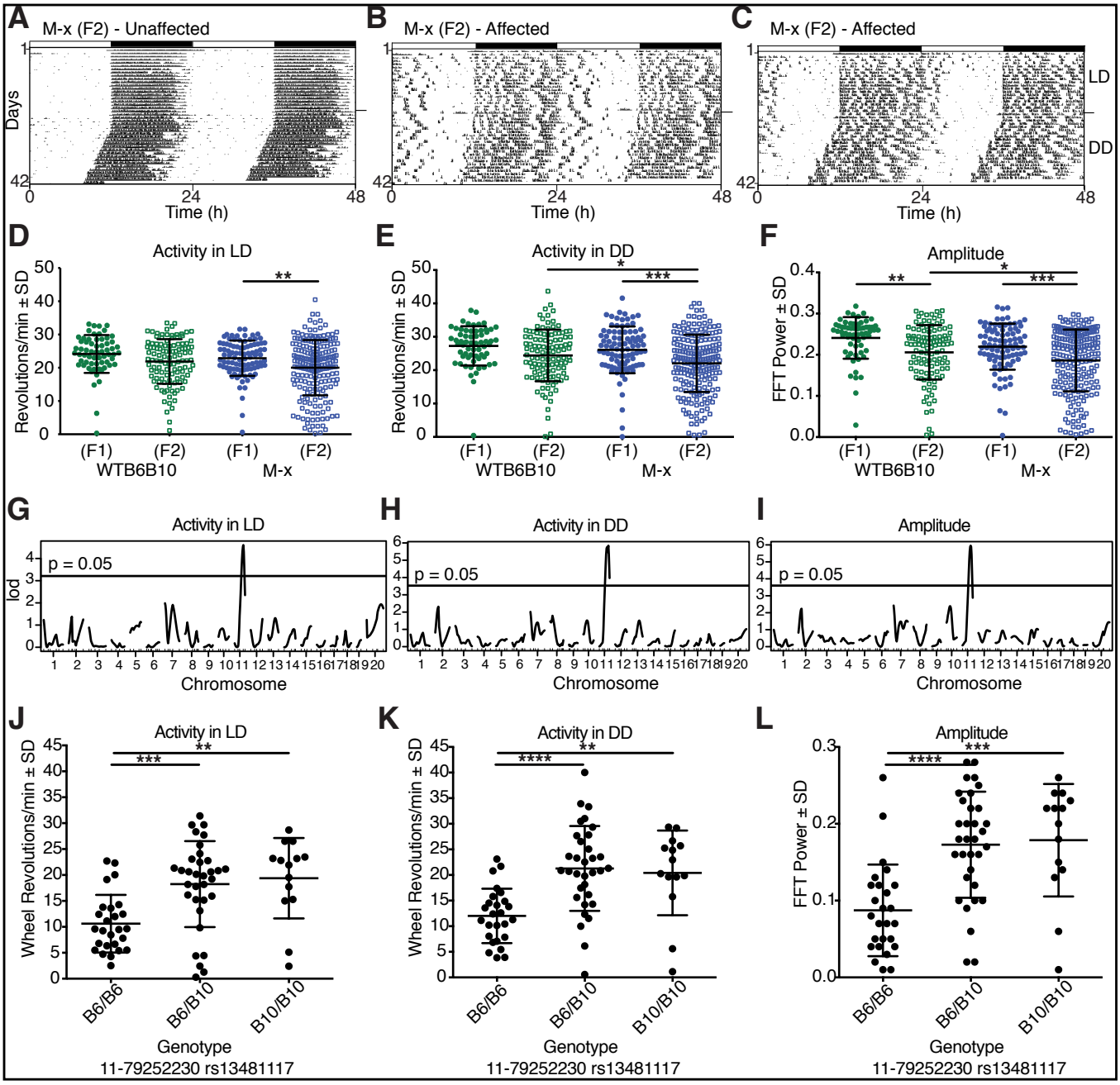
A
M-x (F2) - Unaffected
B
M-x (F2) - Affected
C
M-x (F2) - Affected
Days
LD
DD
Time (h)
D
Activity in LD
Revolutions/min ± SD
(F1)
(F2)
WTB6B10
M-x
E
Activity in DD
F
Amplitude
FFT Power ± SD
G
Activity in LD
lod
p = 0.05
Chromosome
H
Activity in DD
I
Amplitude
J
Activity in LD
Wheel Revolutions/min ± SD
B6/B6
B6/B10
B10/B10
Genotype
11-79252230 rs13481117
K
Activity in DD
L
Amplitude

Figure 4

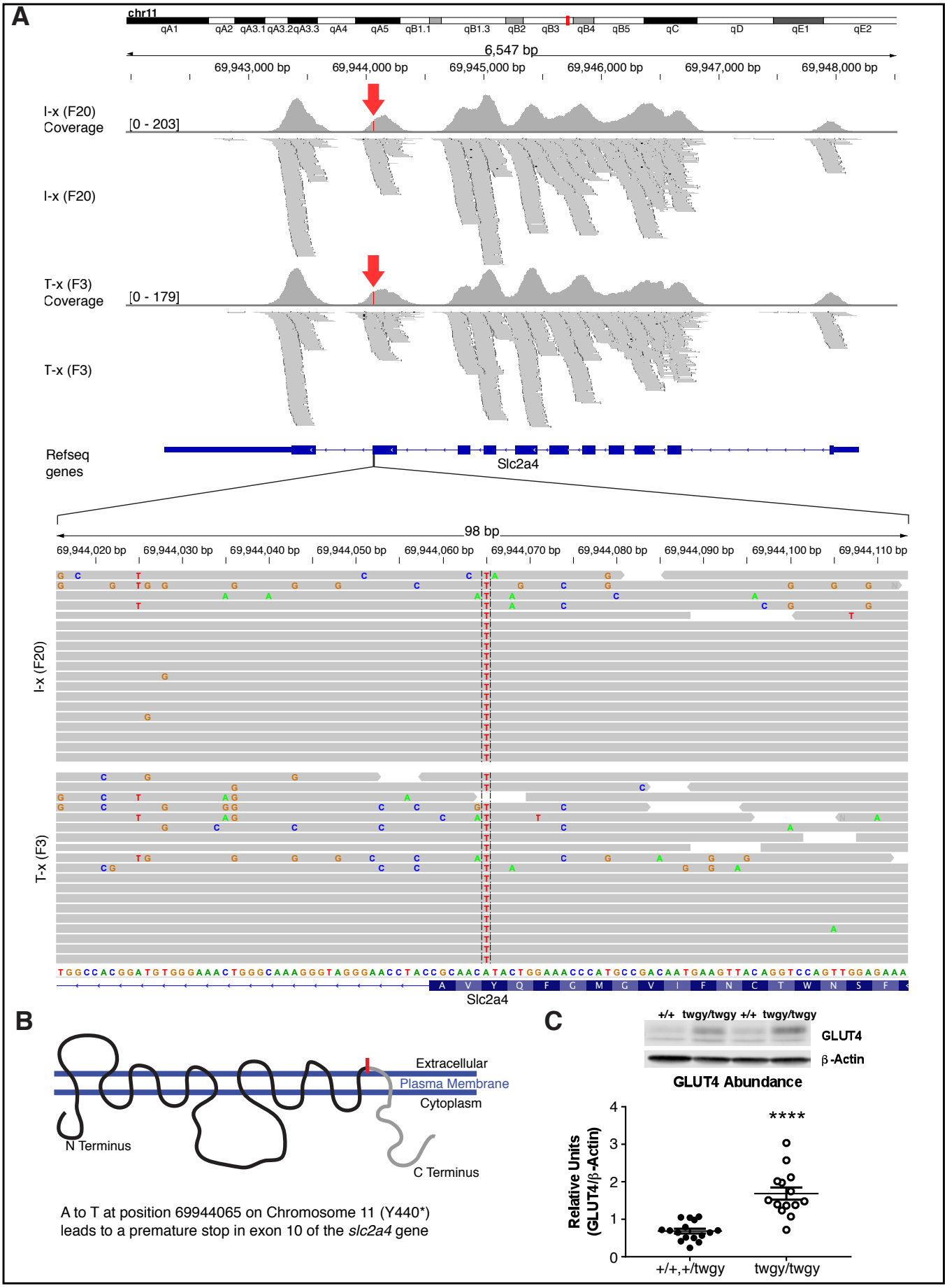
A
chr11
qA1 qA2 qA3.1 qA3.2 qA3.3 qA4 qA5 qB1.1 qB1.3 qB2 qB3 qB4 qB5 qC qD qE1 qE2
6,547 bp
69,943,000 bp
69,944,000 bp
69,945,000 bp
69,946,000 bp
69,947,000 bp
69,948,000 bp
I-x (F20) Coverage
[0 - 203]
I-x (F20)
T-x (F3) Coverage
[0 - 179]
T-x (F3)
Refseq genes
Slc2a4
98 bp
69,944,020 bp
69,944,030 bp
69,944,040 bp
69,944,050 bp
69,944,060 bp
69,944,070 bp
69,944,080 bp
69,944,090 bp
69,944,100 bp
69,944,110 bp
I-x (F20)
T-x (F3)
TGGCCACGGATGTGGGAAACTGGGCAAAGGGTAGGGAACCTACCGCAACATACTGGAAACCCATGCCGACAATGAAGTTACAGGTCCAGTTGGAGAAA
A V Y Q F G M G V I F N C T W N S F
Slc2a4
B
Extracellular
Plasma Membrane
Cytoplasm
N Terminus
C Terminus
A to T at position 69944065 on Chromosome 11 (Y440*)
leads to a premature stop in exon 10 of the slc2a4 gene
C
+/+ twgy/twgy +/+ twgy/twgy
GLUT4
β-Actin
GLUT4 Abundance
Relative Units (GLUT4/β-Actin)
****
0
1
2
3
4
+/+,+/twgy
twgy/twgy

Figure 5

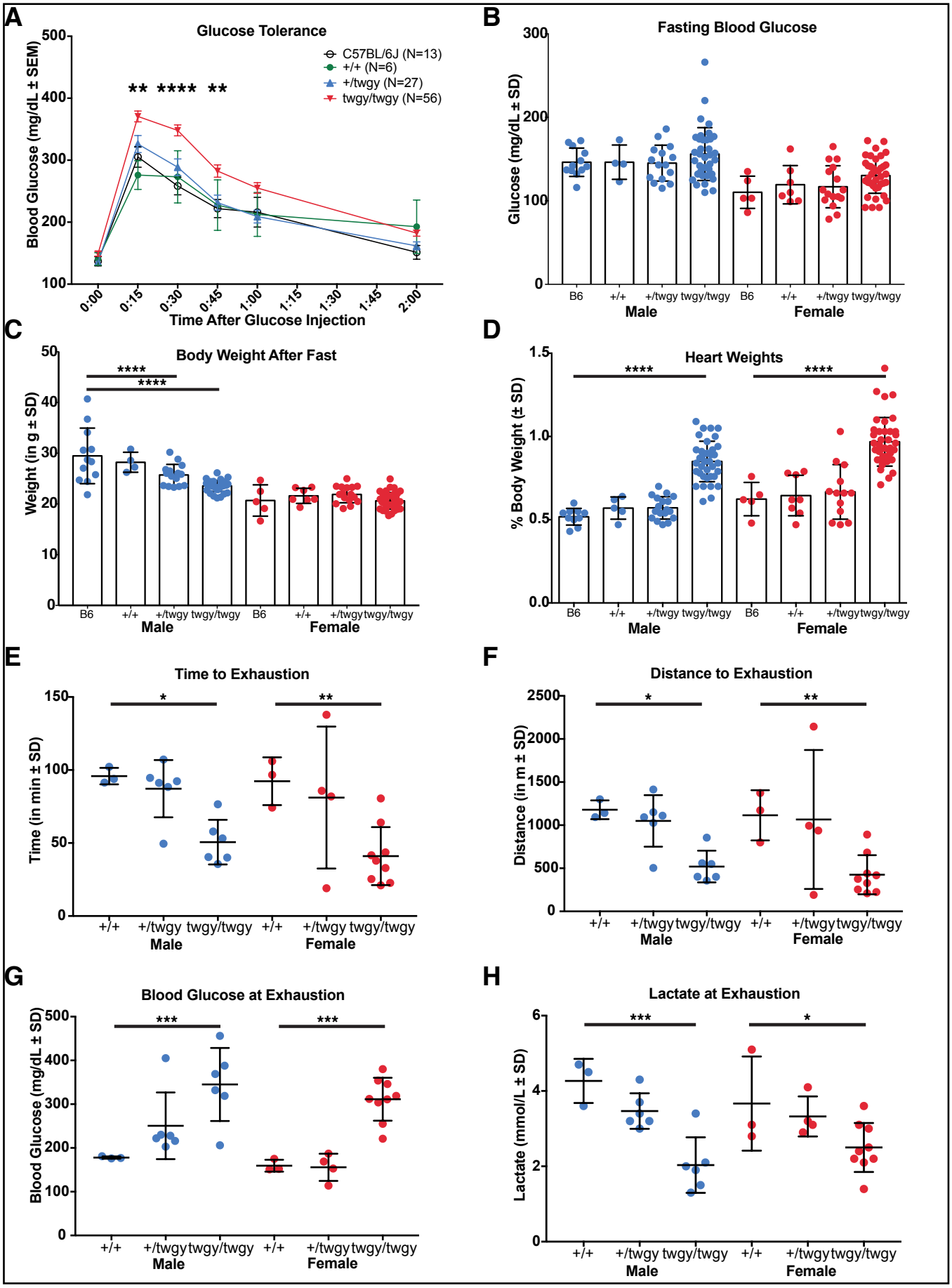
A
Glucose Tolerance
C57BL/6J (N=13)
+/+ (N=6)
+/twgy (N=27)
twgy/twgy (N=56)
** **** **
Blood Glucose (mg/dL ± SEM)
Time After Glucose Injection
B
Fasting Blood Glucose
Glucose (mg/dL ± SD)
B6 +/+ +/twgy twgy/twgy B6 +/+ +/twgy twgy/twgy
Male
Female
C
Body Weight After Fast
Weight (in g ± SD)
D
Heart Weights
% Body Weight (± SD)
E
Time to Exhaustion
Time (in min ± SD)
F
Distance to Exhaustion
Distance (in m ± SD)
G
Blood Glucose at Exhaustion
Blood Glucose (mg/dL ± SD)
H
Lactate at Exhaustion
Lactate (mmol/L ± SD)

Figure 6

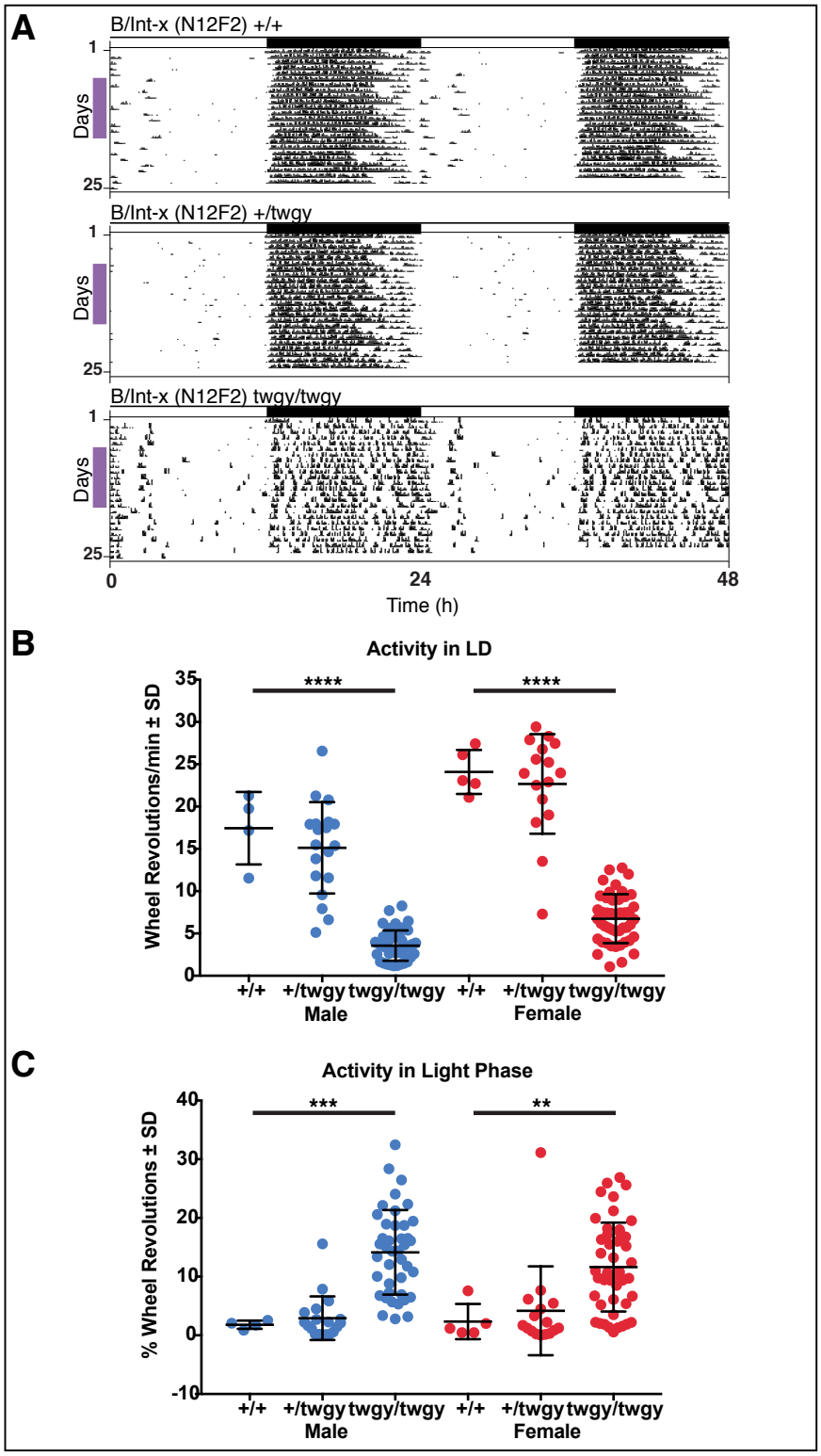
A
B/Int-x (N12F2) +/+
B/Int-x (N12F2) +/twgy
B/Int-x (N12F2) twgy/twgy
Days
1
25
0
24
48
Time (h)
B
Activity in LD
Wheel Revolutions/min ± SD
****
****
+/+
+/twgy
twgy/twgy
Male
Female
C
Activity in Light Phase
% Wheel Revolutions ± SD
***
**

Figure 7